5-2013

Analytical evaluation of adaptive transmission protocols for Markov models of channels with fading and moderate shadowing

Sneha latha Kottapalli
Clemson University, sneha.kottapalli@gmail.com

Analytical Evaluation of Adaptive Transmission Protocols for Markov Models of Channels with Fading and Moderate Shadowing

---

A Thesis
Presented to
the Graduate School of
Clemson University

In Partial Fulfillment
of the Requirements for the Degree
Master of Science
Electrical Engineering

---

by
Sneha L. Kottapalli
May 2013

Accepted by:
Dr. Michael B. Pursley, Committee Chair
Dr. Daniel L. Noneaker
Dr. Harlan B. Russell

Abstract

Adaptive transmission protocols are often employed to communicate over wireless channels with fading and other time-varying propagation losses. The protocols compensate for the propagation losses and maintain high throughput by adjusting transmission parameters in response to the channel variations. Performance evaluations for practical adaptive transmission protocols typically require simulation of both the time-varying processes and the procedure by which the protocol derives information about the channel quality. In this thesis, we develop an analytical method to evaluate the performance of two practical protocols, an adaptive coding protocol and an adaptive modulation and coding protocol, which rely on statistics derived from the demodulation process. Our method for performance analysis avoids the need for simulations of the adaptive protocols and the derivation of statistics that are used for adaptation; furthermore, our approach avoids the simulation of the time-varying channel.

Dedication

To my parents, Yashoda and Nagaraja, my brother, Venky, and my fiancé, Karthik.

Acknowledgments

I sincerely thank my advisor, Dr. Michael B. Pursley, for patiently guiding me through every step of my graduate education. I am fortunate to have been his student and I thank him for all the support and encouragement he has given me. I extend my thanks to Dr. Daniel L. Noneaker and Dr. Harlan B. Russell for serving on my committee. All my committee members have been a great source of inspiration and I thank them for their belief in my capabilities. I am forever grateful for the financial support offered by the Department of Electrical Engineering that enabled me to embark on my graduate studies.

I thank all the students of the CommNets research group for maintaining an engaging and enjoyable research environment. Special thanks to my collaborators, Jason and Michael, for their generous help and valuable inputs.

Sincere thanks to all my roommates and friends at Clemson for helping me find a home away from home. They were a crucial part of my support network.

Finally, I would like to thank my parents for their unconditional love and support that has helped me get this far. Last but not the least, I thank my fiancé, Karthik, who has helped me in more ways than I can recount here. His love, encouragement, and rock-solid support has helped me sail through the roughest of patches. I eagerly look forward to the next phase of our journey together.

Table of Contents

List of Tables

List of Figures

Chapter 1

Introduction

Communication over wireless channels typically suffers from fading and other time-varying propagation losses. Adaptive transmission protocols are employed to achieve high throughput on such channels. The basic premise is to adapt transmission parameters such as modulation and error-control coding in response to the variations in the channel. Several adaptation strategies [1–4] assume that perfect channel-state information is either readily available at the transmitter or relayed back to the transmitter at the same time as the forward transmission. Other adaptive protocols employ pilot or training symbols to estimate the channel state (e.g., [5] and several IEEE standards). In contrast, [6] and [7] have proposed adaptive protocols that rely only on statistics derived from the demodulator and decoder at the receiver. These protocols give nearly optimal performance without requiring full-duplex transmission or the use of pilot symbols; hence, they are more practical.

Performance evaluations of such adaptive transmission protocols typically require extensive simulations. Firstly, the time-varying characteristics of the channel such as fading and shadowing have to be accurately simulated. Finite-state Markov models [8–14] of the channel are often employed to simplify such simulations. Secondly, the operation of the protocol, including the procedure by which it extracts information about the channel

quality, has to be simulated. For the receiver-statistic protocols [6, 7], simulations of the demodulator and decoder, especially an iterative decoder, prove to be time-consuming. Hence, there is a need for analytical evaluation of adaptive transmission protocols that avoids time-consuming simulations. To address this need, analytical methods were given in [14] to determine the performance bounds for adaptive coding on fading channels that are modeled by Markov chains. In [15], the authors derive an analytical approximation to the throughput of an adaptive coding protocol [6] that relies on a count of binary symbol errors.

In this thesis, we build on the work of [14] and [15] to outline an analytical method for evaluating the performance of a general class of adaptive transmission protocols for packet radio systems operating over a time-varying channel. A key aspect in the analytical evaluation of a protocol is the statistical characterization of the process by which the protocol selects transmission parameters for a packet. The analytical method outlined in the thesis can be applied to a general class of adaptive transmission protocols that select transmission parameters for the next packet based on the channel-state information that is derived from measurements, estimates, or statistics obtained from the preceding packet. Our analytical method avoids the need for simulations of the fading process, the shadowing, or the Markov models for these phenomena; furthermore, it avoids simulation of the protocol itself.

We illustrate the analytical method for two protocols, namely, an adaptive coding protocol proposed in [6] and an adaptive modulation and coding protocol investigated in [7]. Both protocols adapt the transmission parameters based on statistics that are derived from the demodulation process. The process by which the protocols select the code or code-modulation combination for a packet can be statistically characterized in terms of the probability distribution of the demodulator statistics. The demodulator statistic for a packet depends on which modulation is employed for the packet. The two adaptive protocols

and the analytical method to evaluate their performance are applicable to many forms of modulation; however, for the purposes of illustration, we consider coherent demodulation of quadriphase shift key (QPSK) modulation, quadrature amplitude modulation (QAM), and biorthogonal modulation. We determine the probability distribution of demodulator statistics that are specific to these modulation formats. The probability distribution is in turn used to statistically characterize the selection process of the protocols.

The thesis is organized as follows. In Chapter 2, a review of the demodulator-statistic based adaptive transmission protocols is provided. The channel model used to evaluate the protocols is given. The modulation formats and the corresponding demodulator statistics that are employed by the protocols are explained. In Chapter 3, we determine the probability distribution of the demodulator statistics. In Chapter 4, we develop the method for performance analysis of the demodulator-statistic based adaptive transmission protocols. As a benchmark for performance, two hypothetical protocols [6, 7] that are given varying degrees of perfect channel-state information are considered. In Chapter 5, the simulation results for the demodulator-statistic based protocols are compared with the analytical calculations for various fading and shadowing scenarios. We also compare the performance of the demodulator-statistic based protocols with that of the hypothetical protocols.

Chapter 2

System Description

We consider packet radio communication systems with half-duplex radios that can adapt transmission parameters on a packet-by-packet basis. In Section 2.1, we give an overview of the adaptive transmission protocols that are considered in this thesis. The channel model is given in Section 2.2. The modulation formats and their corresponding demodulator statistics are given in Sections 2.3 and 2.4 respectively.

2.1 An overview of the protocols

Consider a source that has to send a sequence of packets over a channel with fading and shadowing. The receiver derives information about the channel quality while demodulating and decoding a packet. This information about the channel quality is used by an adaptive protocol to select the transmission parameters for the next packet. The transmission parameters that can be adapted include coding and modulation. The set of error-control codes available at the source is denoted by $\{\mathcal{C}_i : 1 \leq i \leq n_c\}$, indexed in order of increasing rates. The set of modulation formats available at the source is denoted by $\{\mathcal{M}_v : 1 \leq v \leq n_m\}$. The set of code-modulation combinations available at the source is $\{\mathcal{B}_n : 1 \leq n \leq N\}$, for

$N \leq n_c n_m$. In Section 2.1.1, we describe an adaptive coding protocol and in Section 2.1.2, we describe an adaptive modulation and coding protocol.

2.1.1 An adaptive coding protocol

Suppose that the source uses a fixed modulation format and adapts the error-control code in response to the variations in the channel. In this case, $n_m = 1$, $n_c > 1$, $N = n_c$, and $\mathcal{B}_n$ is a combination of the fixed modulation format and code $\mathcal{C}_n$. We consider the adaptive coding protocol proposed in [6] with the modification that the adaptation is based on demodulator statistics (such as those described in Section 2.4).

The adaptive coding protocol selects the code for the next packet by applying an interval test to the demodulator statistic for the preceding packet. The adaptation parameters for the interval test are $\gamma_0, \gamma_1, \ldots, \gamma_{n_c}$ in decreasing order. The adaptation intervals are $\mathcal{I}_n = [\gamma_n, \gamma_{n-1})$ for $1 \leq n \leq n_c$. If the demodulator statistic γ for the preceding packet falls in the interval $\mathcal{I}_n$, then code $\mathcal{C}_n$ is chosen for the next packet. We refer to this protocol as the demodulator-statistic based adaptive coding (AC) protocol.

2.1.2 An adaptive modulation and coding protocol

Suppose that the source is allowed to adapt both the modulation and error-control code in response to the variations in the channel. We consider a variation of the adaptive modulation and coding protocol proposed in [7]. The protocol in [7] uses decoder statistics for adapting the code-modulation combination, and it is restricted to select a combination that is within one step from the combination used for the preceding packet. In our variation, the adaptation is based on demodulator statistics. Further, similar to the AC protocol [6], the adaptive modulation and coding protocol is allowed to choose for the next packet a code-modulation combination that is multiple steps away from the combination used for

the preceding packet.

The adaptive modulation and coding protocol selects a code-modulation combination for the next packet by applying an interval test to the demodulator statistic for the preceding packet. Different modulation formats use different demodulator statistics. The adaptation parameters associated with modulation format $\mathcal{M}_v$ are $\xi_0(v), \xi_1(v), \ldots, \xi_N(v)$ in decreasing order. The adaptation intervals are $\mathcal{I}_{v,n} = [\xi_n(v), \xi_{n-1}(v))$ for $1 \leq n \leq N$. Suppose that the modulation format used for the preceding packet was $\mathcal{M}_v$ and the demodulator statistic was determined to be γ_v. If γ_v falls in the interval $\mathcal{I}_{v,n}$, then combination $\mathcal{B}_n$ is chosen for the next packet. We refer to this protocol as the demodulator-statistic based adaptive modulation and coding (AMC) protocol

2.2 Channel model

We consider time-varying channels that are subject to additive white Gaussian noise (AWGN) with one-sided power spectral density N_0. The time-varying propagation losses in such channels may be due to fading or shadowing. Two independent finite-state Markov chains are used to model the fading and shadowing phenomena.

The parameters of the Markov chain model for fading are derived by the method described in [14]. Each state in the Markov chain corresponds to a propagation loss due to fading. The states of the Markov chain are indexed by $j = 0, 1, \ldots, J_f - 1$. State j represents a propagation loss of $j\Delta_1$ dB above that of state 0, where Δ_1 is the step-size of the Markov chain. The probability of transition from state j to state l in one step is denoted by $q_1(l|j)$. The steady-state probability for state j is denoted by π_j.

A J_s-state Markov chain is used to model shadowing. The states of the Markov chain are indexed by $k = 0, 1, \ldots, J_s - 1$. State k represents a shadow loss of $k\Delta_2$ dB, where Δ_2 is the step-size of the Markov chain. The probability of transition from state k to state m

in one step is denoted by $q_2(m|k)$. The steady-state probability of state k is denoted by π'_k.

The channel is said to be in state (j,k) when the Markov chain for fading is in state j and the Markov chain for shadowing is in state k. The channel state is assumed to be the same for the duration of a packet transmission, but it may change from one packet to the next according to the two Markov chains.

2.3 Modulation formats

The adaptive protocols of Section 2.1 can be employed with many forms of modulation; however, for the purposes of illustration, we consider quadriphase shift key (QPSK) modulation, quadrature amplitude modulation (QAM), and biorthogonal modulation.

Let L_v be the number of modulation symbols in a packet that employs $\mathcal{M}_v$. A packet that employs M-QAM is of the form

$$s(t) = A\sum_{\ell=1}^{L_v}[u_{1,\ell}\cos(\omega t+\phi) - u_{2,\ell}\sin(\omega t+\phi)]p_\tau(t+\tau-\ell\tau), \tag{2.1}$$

where A is the received signal amplitude, ω is the carrier frequency, τ is the individual symbol duration, ϕ is the phase of the signal, $u_{1,\ell}$ and $u_{2,\ell}$ are the data variables on the inphase and quadrature component respectively, and $p_\tau(t)$ is a rectangular pulse of duration τ ($p_\tau(t)=1$ for $0\le t<\tau$ and $p_\tau(t)=0$ for other values of t). The data variables $u_{1,\ell}$ and $u_{2,\ell}$ take values from a set $B=\{\pm1,\pm3,\ldots,\pm K_m\}$, where K_m is an odd positive integer such that $M=(K_m+1)^2$. For $M=4$, (2.1) represents a sequence of L_v QPSK modulated symbols. Likewise, for $M=16$, (2.1) represents a sequence of L_v 16-QAM modulated symbols.

A packet that uses M-ary biorthogonal modulation is of the form

$$s(t) = A\sum_{\ell=1}^{L_v}\psi_\ell(t)p_T(t+T-\ell T), \tag{2.2}$$

where $\psi_\ell(t)$ is a signal from a set of biorthogonal signals of duration $T = K\tau$, where $M = 2K$. For M-ary pulse-coded biorthogonal modulation or M-ary biorthogonal keying (M-BOK), $\psi_\ell(t)$ in (2.2) is of the form

$$\psi_\ell(t) = \sum_{i=1}^{K} u_\ell^{(i)} \cos(\omega t + \phi) p_\tau(t + \tau - i\tau), \tag{2.3}$$

where $\mathbf{u}_\ell = (u_\ell^{(1)}, ..., u_\ell^{(K)})$ is a vector that takes values from a set of M-biorthogonal vectors. We use the rows of a $K \times K$ Hadamard matrix H_K and its complement $-H_K$ as the set of M-biorthogonal vectors.

The rectangular pulse of duration τ is referred to as the *modulation chip*. There is one modulation chip per modulation symbol for M-QAM and there are K modulation chips per modulation symbol for M-BOK. For each modulation format, the chip rate is $1/\tau$, which is proportional to the signal's bandwidth. The chip rate is held constant when the source switches from one modulation format to another; consequently, the bandwidth of the system does not change. The average transmitted power is also held constant, so the best measure of signal-to-noise ratio (SNR) is the chip-energy-to-noise-density ratio defined as $\text{CENR} = 10\log_{10}(\mathcal{E}/N_0)$, where $\mathcal{E}$ is the average energy per modulation chip.

2.4 Demodulator statistics

The adaptive protocols given in Section 2.1 use a statistic that is derived from the demodulation process. The choice of a demodulator statistic for a packet depends on which modulation format is used for the packet. For M-QAM, the demodulator statistic is a distance statistic and for M-ary biorthogonal modulation, the demodulator statistic is a ratio statistic. In the following sections, we briefly describe the demodulation process and explain the statistic that is derived from the process for each modulation format.

2.4.1 Distance statistic

The coherent demodulator for M-QAM modulation may be implemented using matched filters or equivalent correlators in the inphase and quadrature branches. Let $Z_{1,\ell}$ and $Z_{2,\ell}$ denote the ouputs of the correlator in the inphase and quadrature branches, respectively, for the ℓth received symbol. The decision statistic for the ℓth received symbol is $(Z_{1,\ell}, Z_{2,\ell})$, a point in two-dimensional space. When $Z_{1,\ell} = z_{1,\ell}$ and $Z_{2,\ell} = z_{2,\ell}$, we refer to $(z_{1,\ell}, z_{2,\ell})$ as the received point. When the data variable $u_{i,\ell}$ is b_κ, one of the elements of set B defined in Section 2.3, the correlator output $Z_{i,\ell}$ is Gaussian with mean $b_\kappa A\tau/2$ and variance $N_0\tau/4$. For notational convenience, let $\mu = A\tau/2$ and $\sigma^2 = N_0\tau/4$ for the remainder of this thesis.

In the absence of noise, the M possible received points

$$\{(b_\kappa \mu, b_{\kappa'}\mu) : 0 \le \kappa \le K_m, 0 \le \kappa' \le K_m\}$$

are the M symbols that form the output signal constellation. Two nearest neighbors in the constellation are separated by a distance of 2μ. The maximum-likelihood decision is the symbol in the output signal constellation that is closest to the received point. Alternatively, we can view the symbol decision as independent decisions on the inphase and quadrature components. We can view the demodulation of the two-dimensional M-QAM signal as the demodulation of a pair of one-dimensional (K_m+1)-ary amplitude shift keying (ASK) signals [16]. As a result, we use a distance statistic that is based on one-dimensional distances.

In order to obtain the demodulator statistic, the receiver computes $D_{1,\ell}$ and $D_{2,\ell}$, the one-dimensional (1-D) distances for the ℓth received symbol. The 1-D distance $D_{1,\ell}$ for the inphase branch is the minimum of the distances between $z_{1,\ell}$ and the output signal levels $\{-(K_m+1)\mu, \ldots, -\mu, +\mu, \ldots, (K_m+1)\mu)\}$ of (K_m+1)-ary ASK on the inphase component of M-QAM. Similarly, the 1-D distance $D_{2,\ell}$ for the quadrature branch is the

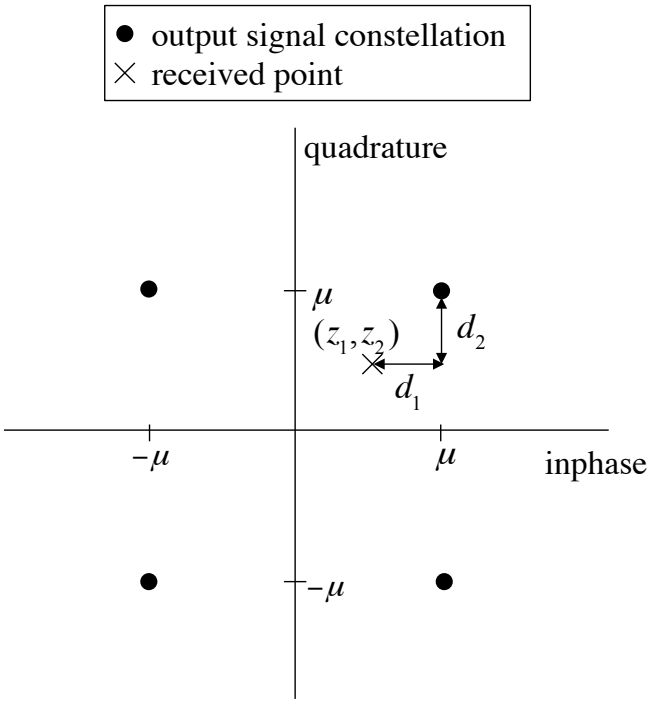

Figure 2.1: Illustration of the 1-D distances for QPSK

minimum of the distances between $z_{2,\ell}$ and the output signal levels of (K_m+1)-ary ASK on the quadrature component. The 1-D distance is

$$D_{i,\ell} = \min\{|Z_{i,\ell} - b_\kappa \mu| : 0 \le \kappa \le K_m\}, \quad i \in \{1,2\}. \tag{2.4}$$

An illustration of the two 1-D distances for a received QPSK symbol is given in Figure 2.1.

The *distance statistic* Γ for a packet is the average of the normalized 1-D distances for all the L_v regular M-QAM modulation symbols in the received packet,

$$\Gamma = \frac{1}{2L_v\mu} \sum_{\ell=1}^{L_v} (D_{1,\ell} + D_{2,\ell}). \tag{2.5}$$

Although the distance statistic is sensitive to the errors in the amplitude and phase references, such errors are typically small in the range of SNR values for which the adaptive

protocol elects to use M-QAM.

2.4.2 Ratio statistic

For M-ary biorthogonal modulation, the maximum-likelihood coherent demodulator may be implemented using K correlators or matched filters. The output sequence of a chip waveform correlator is correlated with each of the K rows of the $K \times K$ Hadamard matrix to give a K-dimensional decision vector $\mathbf{Z}_\ell = (Z_{1,\ell}, Z_{2,\ell}, ..., Z_{K,\ell})$ for the ℓth received symbol [16]. Let $m_1(\mathbf{Z}_\ell)$ and $m_2(\mathbf{Z}_\ell)$ be the decision statistics with the largest and second largest magnitude respectively. For the ℓth received symbol, the receiver calculates the *symbol ratio*

$$R_\ell = \frac{|m_2(\mathbf{Z}_\ell)|}{|m_1(\mathbf{Z}_\ell)|}. \tag{2.6}$$

The symbol ratio was introduced by Viterbi in [17] for anti-jam communications. It was used for soft-decision decoding in [18].

The *ratio statistic* Λ for a packet is the average of the symbol ratios for all the L_v modulation symbols in the packet,

$$\Lambda = \frac{1}{L_v} \sum_{\ell=1}^{L_v} R_\ell. \tag{2.7}$$

The ratio statistic was used to adjust the transmission power of cognitive radios in [7]. It was also used for adapting the code rate in [19].

Chapter 3

Distribution of Demodulator Statistics

In this chapter, we determine the probability distribution of the demodulator statistics for the modulation formats of Section 2.3. The probability distribution is required for the analytical evaluation presented in Chapter 4. In Section 3.1, we determine the distribution of the distance statistic, the demodulator statistic for M-QAM modulation. In Section 3.2, we determine the distribution of the ratio statistic, the demodulator statistic for nonbinary biorthogonal modulation.

The demodulator statistic for a packet depends on the value of CENR when the packet was received. Hence, the distribution of the demodulator statistic varies with the state of the channel. The probability distributions and their parameters (e.g., mean, second moment, and variance) presented in this chapter are conditioned on the channel being in state (j,k). We indicate this dependence on the channel state in the analytical expressions. Also, we compare the values obtained from the analytical expressions with the empirical values obtained from Monte-Carlo simulations in each case.

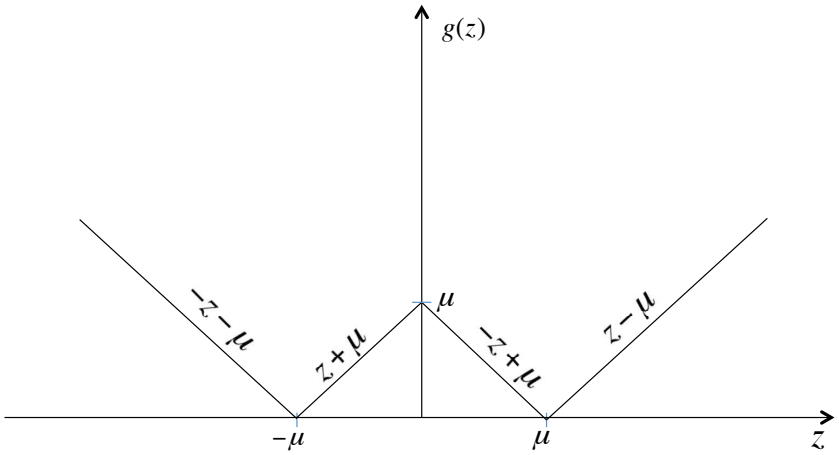

Figure 3.1: The function g for QPSK.

3.1 Distance statistic

For M-QAM, the data variables $U_{1,\ell}$ and $U_{2,\ell}$, $1 \le \ell \le L_v$ are chosen uniformly at random from the set $B = \{b_\kappa : \kappa = 1, 2, \ldots, K_m\}$, where $b_\kappa = K_m - 2\kappa$ and $M = (K_m+1)^2$. For QPSK, the set elements are $b_0 = +1$ and $b_1 = -1$ and for 16-QAM, the elements are $b_0 = +3$, $b_1 = +1$, $b_2 = -1$, and $b_3 = -3$.

The ith 1-D distance ($i = 1, 2$ as M-QAM is a two-dimensional modulation scheme) for the ℓth modulation symbol of any packet can be expressed as a function of the correlator output $Z_{i,\ell}$, $D_{i,\ell} = g(Z_{i,\ell})$, where

$$g(z) = \min\{|z - b_\kappa \mu| : 0 \le \kappa \le K_m\}, \quad -\infty < z < \infty.$$

The function g is shown in Figures 3.1 and 3.2 for QPSK and 16-QAM respectively. By definition, the function g is non-negative and even-symmetric.

We assume that the data variables $U_{1,\ell}$ and $U_{2,\ell}$ are independent. Because the noise components at the output of the inphase and quadrature correlators are statistically independent [16], the correlator outputs $Z_{1,\ell}$ and $Z_{2,\ell}$ are independent. Consequently, the two 1-D distances $D_{1,\ell}$ and $D_{2,\ell}$ are independent. Additionally, we assume that the data vari-

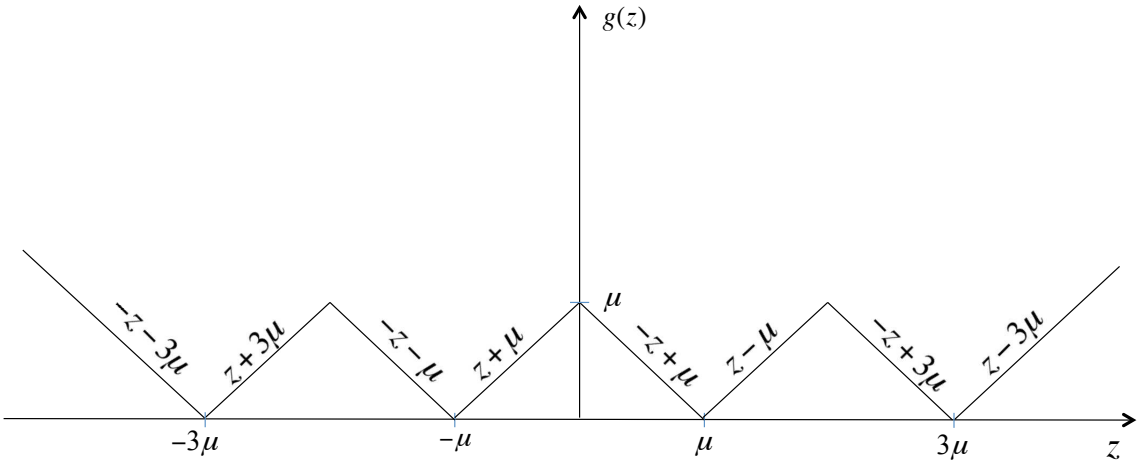

Figure 3.2: The function g for 16-QAM.

ables for a packet, $\{U_{i,\ell} : 1 \le i \le 2, 1 \le \ell \le L_v\}$ are mutually independent and identically distributed (i.i.d.). Recall that the fade level is constant for the duration of a packet transmission and the thermal noise at the receiver is an AWGN process. Hence, the noise components are independent across all symbols in the packet. So, the correlator outputs for a packet, $\{Z_{i,\ell} : 1 \le i \le 2, 1 \le \ell \le L_v\}$ are i.i.d. Therefore, the 1-D distances for a packet, $\{D_{i,\ell} : 1 \le i \le 2, 1 \le \ell \le L_v\}$ are i.i.d.

In Section 3.1.1, we first determine the distribution of the 1-D distance for QPSK and 16-QAM. Then, in Section 3.1.2, we determine the distribution of the distance statistic Γ, which is the average of the sequence of 1-D distances for a packet.

3.1.1 1-D distance distribution

Since all the 1-D distances $D_{i,\ell}$, correlator outputs $Z_{i,\ell}$, and data variables $U_{i,\ell}$ are identically distributed, in all that follows, we use the subscripts i and ℓ only when referring to the sequence of the respective variables corresponding to a packet. Otherwise, we drop the subscripts to simplify the notation.

The cumulative distribution function of the 1-D distance D is

$$F_D(x|j,k) = \sum_{\kappa=0}^{K_m} P(U = b_\kappa) P(g(Z) \leq x|j,k,b_\kappa), \tag{3.1}$$

where $P(g(Z) \leq x|j,k,b_\kappa)$ is the conditional probability that $g(Z) \leq x$ when the channel is in state (j,k) and the data variable U is b_κ. If G_x is the set of all z for which $g(z) \leq x$, then

$$F_D(x|j,k) = \sum_{\kappa=0}^{K_m} \frac{1}{K_m+1} P(Z \in G_x|j,k,b_\kappa). \tag{3.2}$$

Recall that when conditioned on the data variable $U = b_\kappa$, the correlator output Z is Gaussian with mean $b_\kappa\mu$ and variance σ^2, where μ depends on the channel state and σ depends on the thermal noise. For QPSK, $\mu^2/\sigma^2 = \mathcal{E}_{j,k}/N_0$ and for 16-QAM, $\mu^2/\sigma^2 = \mathcal{E}_{j,k}/5N_0$, where $\mathcal{E}_{j,k}$ is the average energy per chip for state (j,k).

In Section 3.1.1.1, we determine the distribution function of the 1-D distance for QPSK by first determining the set G_x and then evaluating the probability that the correlator output Z belongs to this set. In Section 3.1.1.2, we do the same for 16-QAM.

3.1.1.1 QPSK

As the function g is non-negative, the set G_x is empty for $x < 0$. For QPSK, $G_x = [-\mu - x, -\mu + x] \cup [\mu - x, \mu + x]$, for $0 < x \leq \mu$ (Figure 3.3a), and $G_x = [-\mu - x, \mu + x]$, for $x > \mu$ (Figure 3.3b). Without loss of generality, we assume that $U = b_0$ and evaluate the probability that Z belongs to the set G_x. This gives

$$F_D(x|j,k) = \begin{cases} 0, & x \leq 0, \\ \Phi\left(\frac{x-2\mu}{\sigma}\right) + \Phi\left(\frac{x+2\mu}{\sigma}\right) + 2\Phi\left(\frac{x}{\sigma}\right) - 2, & 0 < x \leq \mu, \\ \Phi\left(\frac{x}{\sigma}\right) + \Phi\left(\frac{x+2\mu}{\sigma}\right) - 1, & x > \mu, \end{cases} \tag{3.3}$$

where Φ is the standard Gaussian distribution function.

Using the notation $\varphi(x;a,b) = \frac{\mathrm{d}}{\mathrm{d}x}\Phi\{(x-a)/b\}$, the density function of the 1-D distance for QPSK can be written as

$$f_D(x|j,k) = \begin{cases} 0, & x \leq 0, \\ \varphi(x;2\mu,\sigma) + \varphi(x;-2\mu,\sigma) + 2\varphi(x;0,\sigma), & 0 < x \leq \mu, \\ \varphi(x;0,\sigma) + \varphi(x;-2\mu,\sigma), & x > \mu. \end{cases} \tag{3.4}$$

From inspection, we see that $f_D(x|j,k)$ is bounded for any finite set of nonzero values of σ^2.

The density function given by an analytical expression such as (3.4) is referred to as the *analytical density* in all that follows. For comparison, we also generate a large number of random samples of Z and find the corresponding 1-D distances in order to plot a unit-area histogram of the 1-D distance. The histogram shows relative frequencies of consecutive non-overlapping bins of appropriately chosen size. Such a histogram is referred to as the *empirical density*. The analytical density in (3.4) is compared with the empirical density (bin size $= 0.01$) in Figure 3.4 for three representative values of CENR.

The sharp drop at $x = \mu$ is attributed to the discontinuity in the density function at that point. At $x = \mu$, the density function is

$$f_D(\mu|j,k) = \frac{1}{\sigma\sqrt{2\pi}}\left(3\exp\left\{\frac{-\mu^2}{2\sigma^2}\right\} + \exp\left\{\frac{-9\mu^2}{2\sigma^2}\right\}\right).$$

At $x = \mu^+$, the density function is

$$f_D(\mu^+|j,k) = \frac{1}{\sigma\sqrt{2\pi}}\left(\exp\left\{\frac{-\mu^2}{2\sigma^2}\right\} + \exp\left\{\frac{-9\mu^2}{2\sigma^2}\right\}\right).$$

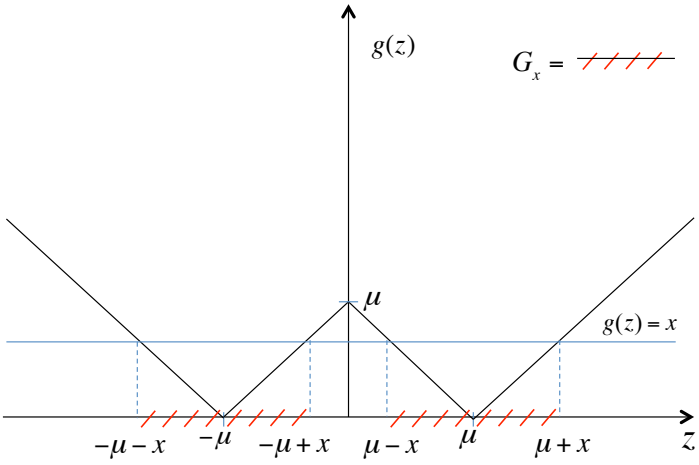

(a) $0 < x \leq \mu$

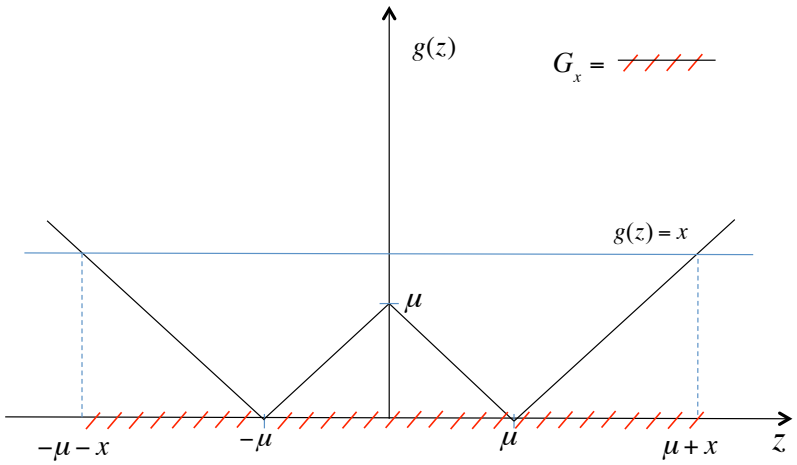

(b) $x > \mu$

Figure 3.3: QPSK: The intervals of z corresponding to G_x for (a) $0 < x \leq \mu$ and (b) $x > \mu$.

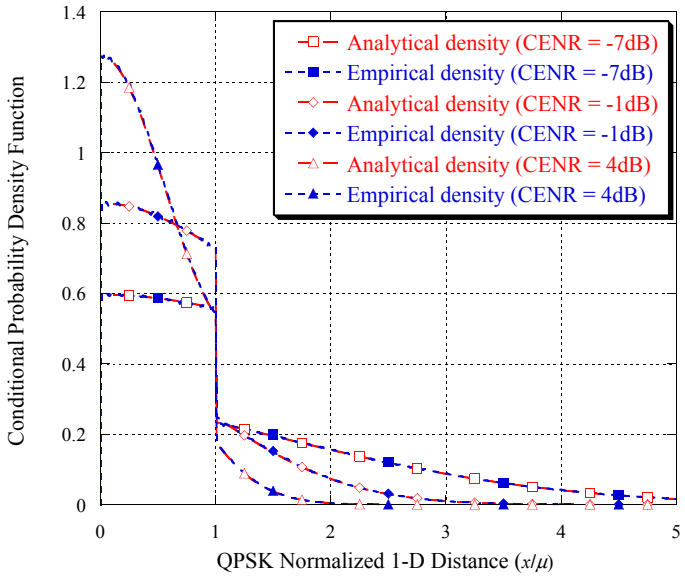

Figure 3.4: QPSK 1-D distance: Comparison of the empirical density and the analytical density for three different values of CENR.

3.1.1.2 16-QAM

For 16-QAM, $G_x = [-3\mu - x, -3\mu + x] \cup [-\mu - x, -\mu + x] \cup [\mu - x, \mu + x] \cup [3\mu - x, 3\mu + x]$ for $0 < x \leq \mu$ (Figure 3.5a) and $G_x = [-3\mu - x, 3\mu + x]$ for $x > \mu$ (Figure 3.5b). The probability that Z belongs to the set G_x can be evaluated to give

$$F_D(x|j,k) = \begin{cases} 0, & x \leq 0, \\ 2\Phi\left(\frac{x}{\sigma}\right) + \frac{3}{2}\Phi\left(\frac{x-2\mu}{\sigma}\right) + \frac{3}{2}\Phi\left(\frac{x+2\mu}{\sigma}\right) + \Phi\left(\frac{x-4\mu}{\sigma}\right) & \\ \quad + \Phi\left(\frac{x+4\mu}{\sigma}\right) + \frac{1}{2}\Phi\left(\frac{x-6\mu}{\sigma}\right) + \frac{1}{2}\Phi\left(\frac{x+6\mu}{\sigma}\right) - 4, & 0 < x \leq \mu, \\ \frac{1}{2}\left[\Phi\left(\frac{x}{\sigma}\right) + \Phi\left(\frac{x+2\mu}{\sigma}\right) + \Phi\left(\frac{x+4\mu}{\sigma}\right) + \Phi\left(\frac{x+6\mu}{\sigma}\right)\right] - 1, & x > \mu. \end{cases} \tag{3.5}$$

The derivation of (3.5) is given in Appendix A.

The density function of the 1-D distance for 16-QAM is given by

$$f_D(x|j,k) = \begin{cases} 0, & x \leq 0, \\ 2\varphi(x;0,\sigma) + \frac{3}{2}\varphi(x;2\mu,\sigma) + \frac{3}{2}\varphi(x;-2\mu,\sigma) + \varphi(x;4\mu,\sigma) & \\ \quad +\varphi(x;-4\mu,\sigma) + \frac{1}{2}\varphi(x;6\mu,\sigma) + \frac{1}{2}\varphi(x;-6\mu,\sigma), & 0 < x \leq \mu, \\ \frac{1}{2}\left(\varphi(x;0,\sigma) + \varphi(x;-2\mu,\sigma) + \varphi(x;-4\mu,\sigma) + \varphi(x;-6\mu,\sigma)\right), & x > \mu. \end{cases} \tag{3.6}$$

The analytical density in (3.6) is compared with the empirical density (with bin size $=0.01$) for three representative values of CENR in Figure 3.6. The sharp drop at $x=\mu$ is attributed to the discontinuity in the density function at that point. At $x=\mu$, the density function is

$$f_D(\mu|j,k) = \frac{1}{\sigma\sqrt{8\pi}}\left(7\exp\left\{\frac{-\mu^2}{2\sigma^2}\right\} + 5\exp\left\{\frac{-9\mu^2}{2\sigma^2}\right\} + 3\exp\left\{\frac{-25\mu^2}{2\sigma^2}\right\} + \exp\left\{\frac{-49\mu^2}{2\sigma^2}\right\}\right).$$

At $x=\mu^+$, the density function is

$$f_D(\mu^+|j,k) = \frac{1}{\sigma\sqrt{8\pi}}\left(\exp\left\{\frac{-\mu^2}{2\sigma^2}\right\} + \exp\left\{\frac{-9\mu^2}{2\sigma^2}\right\} + 2\exp\left\{\frac{-25\mu^2}{2\sigma^2}\right\}\right).$$

3.1.2 Distribution of distance statistic

We are primarily interested in the distribution of the distance statistic Γ, average of the i.i.d. sequence of normalized 1-D distances for a packet. One possible approach to obtain the exact density of Γ is to carry out a $2L_v$-fold convolution of the density function of D with itself [20]. An alternative approach is to find the $2L_v$th power of the moment generating function of D and take its inverse Fourier transform. Both the approaches fail to give a closed-form expression for the distribution of Γ.

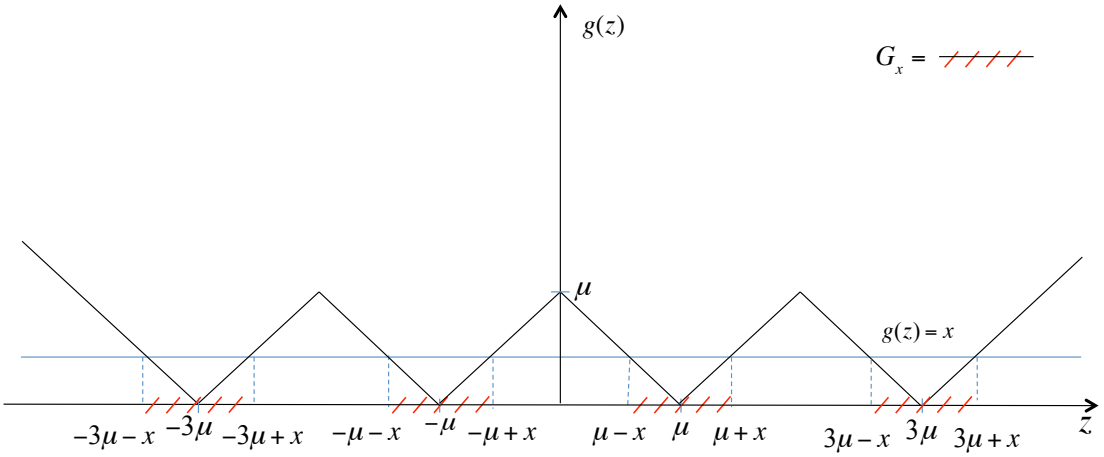

(a) $0 < x \leq \mu$

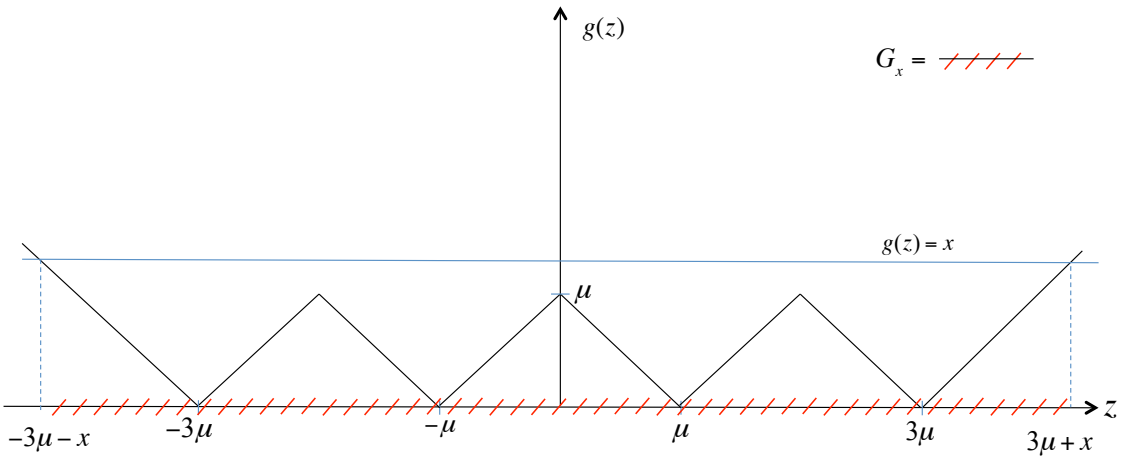

(b) $x > \mu$

Figure 3.5: 16-QAM: The intervals of z corresponding to G_x for (a) $0 < x \leq \mu$ and (b) $x > \mu$.

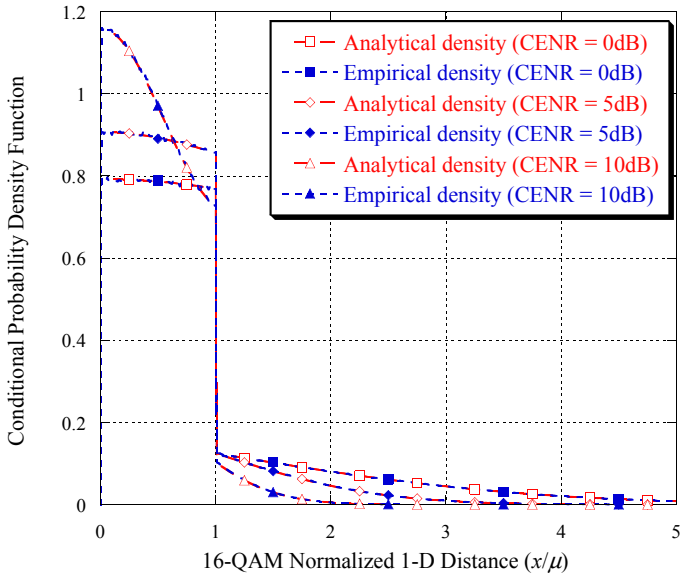

Figure 3.6: 16-QAM 1-D distance: Comparison of the empirical density and the analytical density for three different values of CENR.

However, we observe that the central limit theorem can be used to obtain a good approximation for the distribution of the distance statistic. Recall that the distance statistic is

$$\begin{aligned}\Gamma &= \frac{1}{2L_v\mu}\sum_{\ell=1}^{L_v}(D_{1,\ell}+D_{2,\ell}) \\ &= \frac{1}{2L_v\mu}\sum_{\ell=1}^{L_v}\{g(Z_{1,\ell})+g(Z_{2,\ell})\}. \end{aligned} \tag{3.7}$$

The 1-D distances $\{D_{i,\ell} : 1 \le i \le 2, 1 \le \ell \le L_v\}$ for a packet are i.i.d. with each random variable having both a *finite* mean $\mu_D(j,k)$ and *finite* variance $\sigma_D^2(j,k)$, which is proved shortly. From the central limit theorem, the probability distribution function of the average Γ is approximately a Gaussian distribution function with mean $\mu_D(j,k)/\mu$ and variance $\sigma_D^2(j,k)/2L_v\mu^2$ for large values of L_v.

The mean and the second moment of D are given by

$$E[D|j,k] = \sum_{\kappa=0}^{K_m} P(U = b_\kappa) \int_{-\infty}^{\infty} g(z) f_Z(z|j,k,b_\kappa) dz \tag{3.8}$$

and

$$E[D^2|j,k] = \sum_{\kappa=0}^{K_m} P(U = b_\kappa) \int_{-\infty}^{\infty} g^2(z) f_Z(z|j,k,b_\kappa) dz, \tag{3.9}$$

where $f_Z(z|j,k,b_\kappa)$ is the conditional density of the correlator output when the channel is in state (j,k) and the data variable is b_κ. Evaluation of (3.8) and (3.9) for QPSK (Appendix C) gives

$$\mu_D(j,k) = \sigma\sqrt{\frac{2}{\pi}}\left(1 - e^{\frac{-\mu^2}{2\sigma^2}} + e^{\frac{-2\mu^2}{\sigma^2}}\right) + 2\mu\left\{\Phi\left(\frac{-\mu}{\sigma}\right) - 2\Phi\left(\frac{-2\mu}{\sigma}\right)\right\} \tag{3.10a}$$

and

$$\sigma_D^2(j,k) = \sigma^2 + 4\mu^2\Phi\left(\frac{-\mu}{\sigma}\right) - 2\mu\sigma\sqrt{\frac{2}{\pi}}e^{\frac{-\mu^2}{2\sigma^2}} - [\mu_D(j,k)]^2. \tag{3.10b}$$

Evaluation of (3.8) and (3.9) for 16-QAM (Appendix D) gives

$$\mu_D(j,k) = \frac{\sigma}{\sqrt{2\pi}}\left(2 + \sum_{h=1}^{6}(-1)^h \lceil (7-h)/2 \rceil e^{\frac{-h^2\mu^2}{2\sigma^2}}\right) + \mu\sum_{h=1}^{6} h(-1)^{h+1} \lceil (7-h)/2 \rceil \Phi\left(\frac{-h\mu}{\sigma}\right) \tag{3.11a}$$

and

$$\begin{aligned}\sigma_D^2(j,k) = {} & \sigma^2 - \frac{\mu\sigma}{2\sqrt{2\pi}}(13e^{\frac{-\mu^2}{2\sigma^2}} + 8e^{\frac{-9\mu^2}{2\sigma^2}} + 4e^{\frac{-25\mu^2}{2\sigma^2}}) \\ & + 2\mu^2\left[3\Phi\left(\frac{-\mu}{\sigma}\right) + 6\Phi\left(\frac{-3\mu}{\sigma}\right) + 5\Phi\left(\frac{-5\mu}{\sigma}\right)\right] - [\mu_D(j,k)]^2.\end{aligned} \tag{3.11b}$$

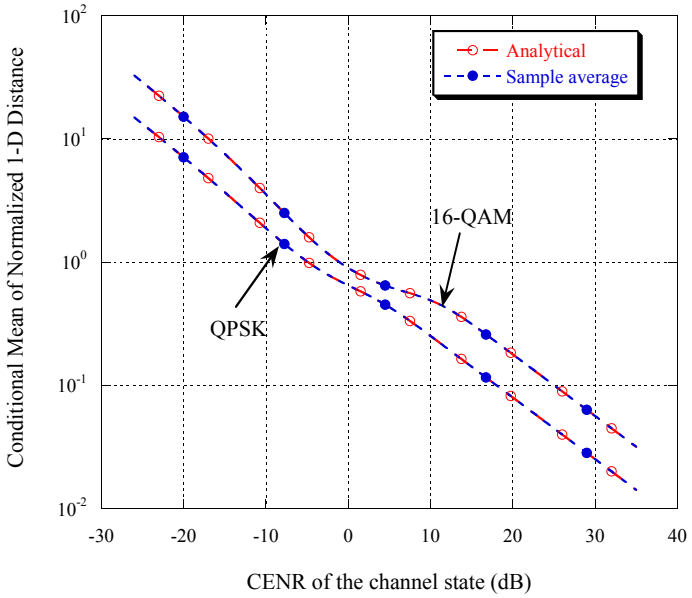

Figure 3.7: Comparison of the analytical mean and the sample average of the 1-D distances for QPSK and 16-QAM as a function of CENR.

We note that the mean and the variance of 1-D distance are finite for both QPSK and 16-QAM. The mean and variance values that are given by (3.10) and (3.11) are referred to as the *analytical mean* and *analytical variance*. For comparison, we generate a large number of random samples of the 1-D distance, find the sample average and the sample variance, and plot the results in Figures 3.7 and 3.8.

The convergence of the distribution function does not always guarantee the convergence of the density function to the Gaussian density [21]. However, the 1-D distance has properties that guarantee convergence of the density function as well. The 1-D distance, for both QPSK and 16-QAM, has a finite second moment (proved in Appendices C and D). Also, the probability density function of the 1-D distance is bounded (Sections 3.1.1.1 and 3.1.1.2). By the local limit theorem for densities (see §46 in [21] and Chapter VII.2 in [22]), the density function of the average Γ is approximately a Gaussian density with mean $\mu_D(j,k)/\mu$ and variance $\sigma_D^2(j,k)/2L_v\mu^2$ for large values of L_v. The empirical den-

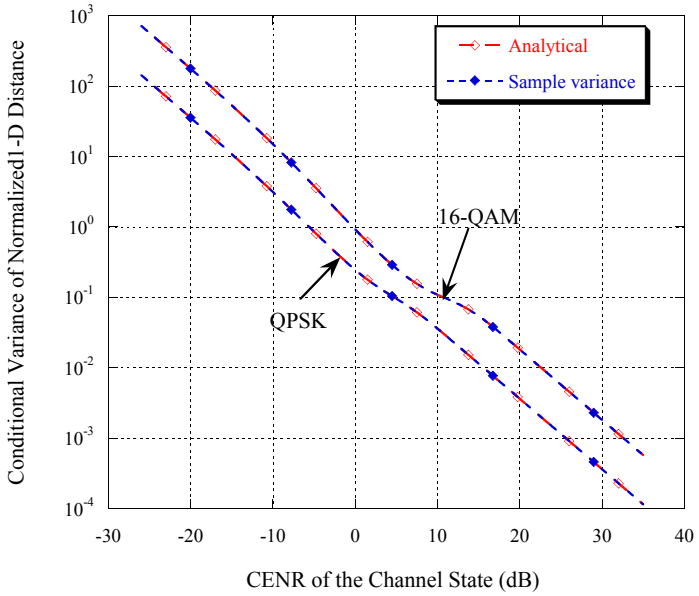

Figure 3.8: Comparison of the analytical variance and the sample variance of the 1-D distances for QPSK and 16-QAM as a function of CENR.

sity of the distance statistic is compared with the Gaussian approximation for QPSK and 16-QAM in Figures 3.9 and 3.10 respectively.

3.2 Ratio statistic

Recall that the symbol ratio for the ℓth received symbol of a packet that uses M-BOK is

$$R_\ell = \frac{|m_2(\mathbf{Z}_\ell)|}{|m_1(\mathbf{Z}_\ell)|},$$

where $m_1(\mathbf{Z}_\ell)$ is the decision statistic with the largest magnitude and $m_2(\mathbf{Z}_\ell)$ is the decision statistic with the second largest magnitude. Here, R_ℓ is well-defined only when $|m_1(\mathbf{Z}_\ell)|$ is non-zero. The event $m_1(\mathbf{Z}_\ell) = 0$ is equivalent to the vector of decision statistics, $\mathbf{Z}_\ell = (Z_{1,\ell}, Z_{2,\ell}, ..., Z_{K,\ell})$ being zero; hence, it occurs with zero probability. Therefore, we may assume that the symbol ratio R_ℓ is well-defined and takes values in the range $[0,1]$. We

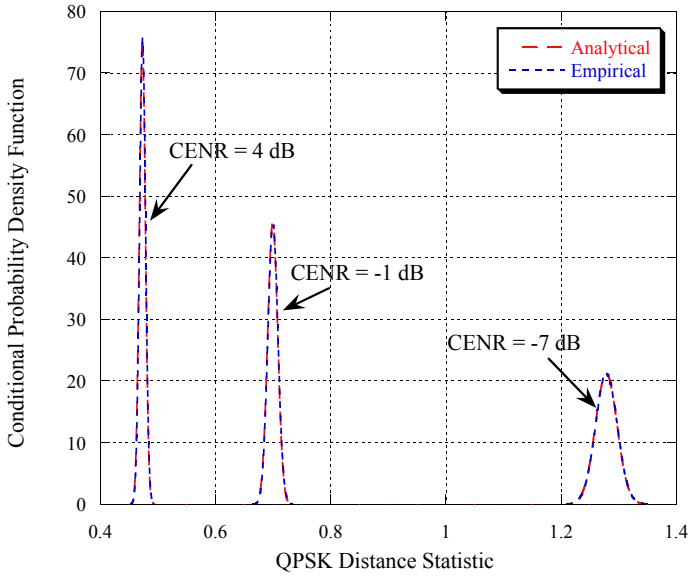

Figure 3.9: QPSK distance statistic: Comparison of the analytical density and the empirical density for three different values of CENR when $L_v = 2048$.

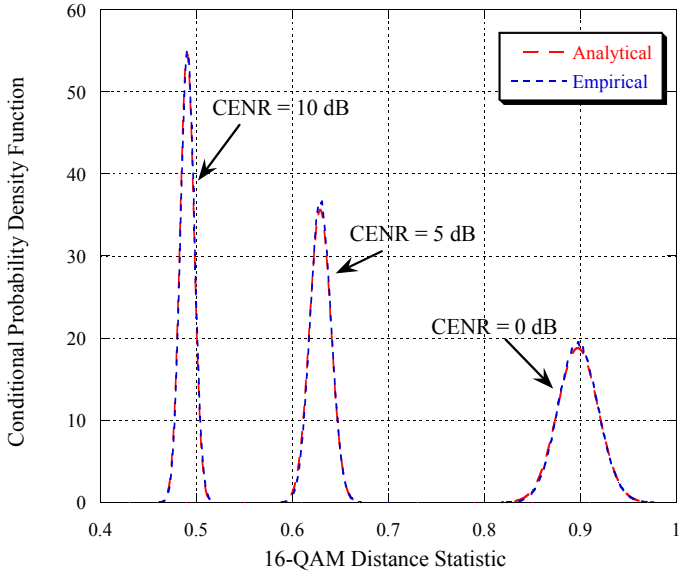

Figure 3.10: 16-QAM distance statistic: Comparison of the analytical density and the empirical density for three different values of CENR when $L_v = 1024$.

assume that the sequence of modulation symbols in a packet is i.i.d.; hence, the symbol ratios $\{R_\ell : 1 \le \ell \le L_v\}$ are i.i.d. Further, the symbol ratios $\{R_\ell : 1 \le \ell \le L_v\}$ have both a finite mean $\mu_R(j,k)$ and finite variance $\sigma_R^2(j,k)$, since each R_ℓ is bounded.

Recall that the ratio statistic for a packet is the average of the sequence of symbol ratios for the packet. By the central limit theorem, the probability distribution function of the ratio statistic converges to the Gaussian distribution with mean $\mu_R(j,k)$ and variance $\sigma_R^2(j,k)/L_v$ for large values of L_v.

The mean $\mu_R(j,k)$ and the variance $\sigma_R^2(j,k)$ can both be expressed in terms of the multivariate density of $\mathbf{Z}_\ell$. Suppose that symbol ζ_1 from the M-BOK signal set

$$\{-\zeta_K, \ldots, -\zeta_1, \zeta_1, \ldots, \zeta_K\}$$

is sent as the ℓth modulation symbol. Conditioned on ζ_1 being sent, the decision statistics $Z_{1,\ell}, Z_{2,\ell}, ..., Z_{K,\ell}$ are mutually independent Gaussian random variables with variance $N_0T/4$. The mean of $Z_{1,\ell}$ (the decision statistic that corresponds to the transmitted symbol) is $AT/2$, while the mean of the remaining decision statistics is zero. The conditional mean of the symbol ratio when ζ_1 is sent is

$$E\left[\left.\frac{|m_2(\mathbf{Z}_\ell)|}{|m_1(\mathbf{Z}_\ell)|}\right| j,k,\zeta_1\right] = \int_{-\infty}^{\infty}\cdots\int_{-\infty}^{\infty}\frac{|m_2(\mathbf{z})|}{|m_1(\mathbf{z})|}\frac{1}{(\pi N_0T/2)^{K/2}}\mathrm{e}^{-\frac{(z_1-AT/2)^2+\sum_{i=2}^{K}z_i^2}{N_0T/2}}dz_1\ldots dz_K.$$

From this expression, we see that the mean of the symbol ratio does not depend on the symbol that was sent. Hence,

$$\begin{aligned}\mu_R(j,k) =& E\left[\left.\frac{|m_2(\mathbf{Z}_\ell)|}{|m_1(\mathbf{Z}_\ell)|}\right| j,k\right] = E\left[\left.\frac{|m_2(\mathbf{Z}_\ell)|}{|m_1(\mathbf{Z}_\ell)|}\right| j,k,\zeta_1\right]\\ =& \int_{-\infty}^{\infty}\cdots\int_{-\infty}^{\infty}\frac{|m_2(\mathbf{z})|}{|m_1(\mathbf{z})|}\frac{1}{(\pi N_0T/2)^{K/2}}\mathrm{e}^{-\frac{(z_1-AT/2)^2+\sum_{i=2}^{K}z_i^2}{N_0T/2}}dz_1\ldots dz_K. \qquad (3.12)\end{aligned}$$

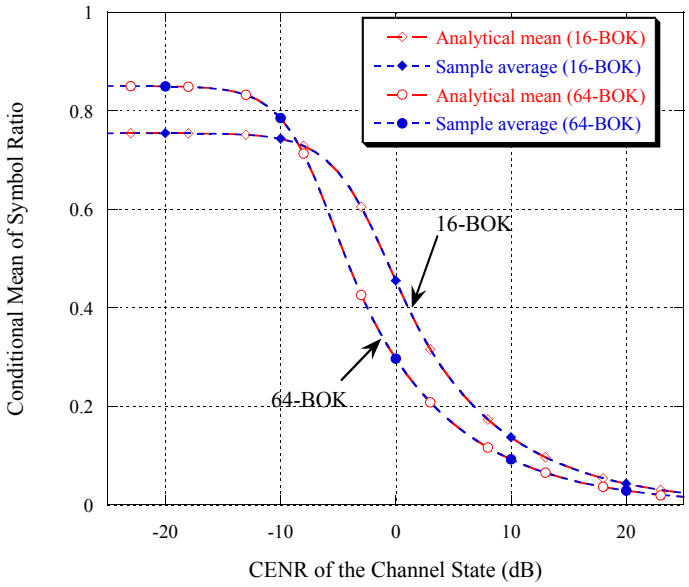

Figure 3.11: Comparison of the analytical mean and sample average of the symbol ratio for 16-BOK and 64-BOK as a function of CENR.

Similarly,

$$\sigma_R^2(j,k) = \left(\int_{-\infty}^{\infty} \cdots \int_{-\infty}^{\infty} \left(\frac{|m_2(\mathbf{z})|}{|m_1(\mathbf{z})|} \right)^2 \frac{1}{(\pi N_0 T/2)^{K/2}} \mathrm{e}^{-\frac{(z_1 - AT/2)^2 + \sum_{i=2}^{K} z_i^2}{N_0 T/2}} dz_1 \ldots dz_K \right) - [\mu_R(j,k)]^2. \tag{3.13}$$

In general, the integrals in (3.12) and (3.13) cannot be evaluated in closed-form. The K-dimensional integrals in (3.12) and (3.13) can be expressed in terms of repeated one-dimensional integrals (Appendix E) that can be evaluated using numerical integration. The mean values obtained from numerical integration are compared with the sample averages for 16-BOK and 64-BOK in Figure 3.11. Likewise, the comparison for the variance is shown in Figure 3.12.

Additionally, we can quantify the rate at which the probability distribution of the ratio statistic converges to the Gaussian distribution as L_v increases. We can bound the error

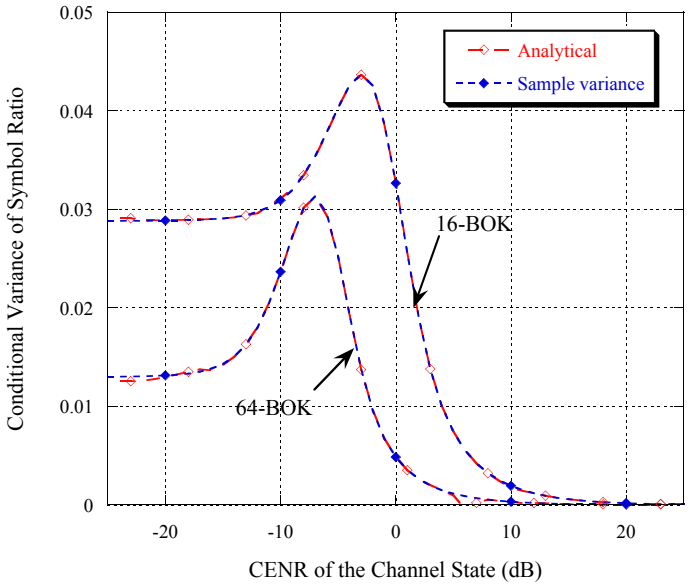

Figure 3.12: Comparison of the analytical variance and sample variance of the symbol ratio for 16-BOK and 64-BOK as a function of CENR.

in the Gaussian approximation by the Berry-Esseen theorem [21,23]. Since $E[|R_\ell|^3] \leq 1$ for each ℓ, we can guarantee that for all x

$$\left| F_\Lambda(x|j,k) - \Phi\left(\frac{x - \mu_R(j,k)}{\sigma_R(j,k)/\sqrt{L_v}} \right) \right| \leq \frac{c}{\sqrt{L_v}}, \tag{3.14}$$

where c is a constant.

Chapter 4

Performance Analysis of Adaptive Transmission Protocols

When a source must send a sequence of packets to a destination over the duration of a *session*, it adapts the transmission parameters on a packet-by-packet basis according to the adaptive protocol. We evaluate the performance of the adaptive transmission protocol by measuring the average throughput for a session. In Section 4.1, we define session throughput and give the analytical expressions for evaluating the average throughput of the demodulator-statistic based adaptive transmission protocols for the Markov models of the fading channel and shadowing. In Section 4.2, we consider two hypothetical protocols that are given perfect information about the channel state. The hypothetical protocols provide benchmarks for the performance of the adaptive transmission protocols.

4.1 Session throughput

Each packet represents N_b binary code symbols. Consequently, the number of modulation chips and the number of modulation symbols (L_v) in a packet depend on the mod-

ulation format used for the packet. Since the chip rate is held constant, the use of multiple modulation formats requires packets of variable duration. To account for this, we define the standard *time unit* to be the duration of a packet that uses QPSK. We say that an information bit is *delivered* if the packet that contains the bit is decoded correctly. The *session throughput* for an adaptive transmission protocol is defined as the average number of information bits delivered per unit of time the source is transmitting packets.

Let $N_t[n]$ be the number of time units required to transmit a packet that uses code-modulation combination $\mathcal{B}_n$. Let $r[n]$ be the rate of the error-control code employed by $\mathcal{B}_n$. The number of information bits in a packet that uses $\mathcal{B}_n$ is $r[n]N_b$. Let $s(n|l,m)$ be the average number of information bits delivered per time unit by a packet that uses combination $\mathcal{B}_n$ and is sent when the channel is in state (l,m). Then, $s(n|l,m)$ is given by

$$s(n|l,m) = \frac{r[n]N_b P_c(n|l,m)}{N_t[n]}, \tag{4.1}$$

where $P_c(n|l,m)$ is the probability of correctly decoding a packet that uses combination $\mathcal{B}_n$ when the channel is in state (l,m). The average number of information bits delivered by a packet that uses $\mathcal{B}_n$ is

$$r[n]N_b P_c(n|l,m) = s(n|l,m)N_t[n]. \tag{4.2}$$

We consider a general class of adaptive transmission protocols that select a code-modulation combination for the next packet based on the preceding channel state. The selection process of such protocols can be statistically characterized by $\mathcal{Q}(n|j,k)$, the conditional probability that the protocol selects $\mathcal{B}_n$ for the next packet given that the channel was in state (j,k) for the preceding packet. For any such adaptive transmission protocol,

the average number of information bits delivered per packet transmission is

$$N_I = \sum_{n=1}^{N} \sum_{l=0}^{J_f-1} \sum_{m=0}^{J_s-1} r[n] N_b P_c(n|l,m) \sum_{j=0}^{J_f-1} \sum_{k=0}^{J_s-1} \mathcal{Q}(n|j,k) q_1(l|j) q_2(m|k) \pi_j \pi'_k$$
$$= \sum_{n=1}^{N} \sum_{l=0}^{J_f-1} \sum_{m=0}^{J_s-1} s(n|l,m) N_t[n] \sum_{j=0}^{J_f-1} \sum_{k=0}^{J_s-1} \mathcal{Q}(n|j,k) q_1(l|j) q_2(m|k) \pi_j \pi'_k. \tag{4.3}$$

The average number of time units per packet that the source is transmitting during a session is

$$N_T = \sum_{n=1}^{N} N_t[n] \sum_{j=0}^{J_f-1} \sum_{k=0}^{J_s-1} \mathcal{Q}(n|j,k) \pi_j \pi'_k. \tag{4.4}$$

Then, for the protocol the session throughput for the Markov chain models of the fading channel and shadowing described in Section 2.2 is

$$S = \frac{N_I}{N_T}$$
$$= \frac{\sum_{n=1}^{N} \sum_{l=0}^{J_f-1} \sum_{m=0}^{J_s-1} s(n|l,m) N_t[n] \sum_{j=0}^{J_f-1} \sum_{k=0}^{J_s-1} \mathcal{Q}(n|j,k) q_1(l|j) q_2(m|k) \pi_j \pi'_k}{\sum_{n=1}^{N} N_t[n] \sum_{j=0}^{J_f-1} \sum_{k=0}^{J_s-1} \mathcal{Q}(n|j,k) \pi_j \pi'_k}. \tag{4.5}$$

In Section 4.1.1, we illustrate the analytical method for the AC protocol. In Section 4.1.2, we do the same for the AMC protocol by deriving analytical expressions for $\mathcal{Q}(n|j,k)$.

4.1.1 AC protocol

If a fixed modulation format is employed with adaptive coding, then all packets are of the same duration, so $N_t[n]$ does not depend on n. Hence, the analytical expression for

Code $\mathcal{C}_n$	Code rate	$\mathcal{I}_n$
$\mathcal{C}_1$	0.236	$[0.685, \infty)$
$\mathcal{C}_2$	0.325	$[0.579, 0.685)$
$\mathcal{C}_3$	0.495	$[0.493, 0.579)$
$\mathcal{C}_4$	0.660	$[0.441, 0.493)$
$\mathcal{C}_5$	0.793	$[0, 0.441)$

Table 4.1: The adaptation intervals for the AC protocol with QPSK modulation.

the throughput of the AC protocol simplifies to

$$S_{\mathrm{AC}} = \sum_{n=1}^{n_c} \sum_{l=0}^{J_f-1} \sum_{m=0}^{J_s-1} s(n|l,m) \sum_{j=0}^{J_f-1} \sum_{k=0}^{J_s-1} \mathcal{Q}_{\mathrm{AC}}(n|j,k) q_1(l|j) q_2(m|k) \pi_j \pi'_k. \tag{4.6}$$

The protocol's code selection process is statistically characterized by $\mathcal{Q}_{\mathrm{AC}}(n|j,k)$, the probability that code $\mathcal{C}_n$ is chosen for the next packet given that the preceding channel state was (j,k). Since the AC protocol chooses the code by applying an interval test to the demodulator statistic, $\mathcal{Q}_{\mathrm{AC}}(n|j,k)$ is the probability that the demodulator statistic Γ falls in the interval $\mathcal{I}_n = [\gamma_n, \gamma_{n-1})$ given that the preceding channel state was (j,k); that is

$$\mathcal{Q}_{\mathrm{AC}}(n|j,k) = P(\Gamma \in \mathcal{I}_n | j,k). \tag{4.7}$$

For our numerical results, we employ five binary turbo product codes [24] of rates 0.236, 0.325, 0.495, 0.660, and 0.793 with QPSK modulation. The binary code symbols of a packet are interleaved by an *S*-random interleaver [25] prior to modulation. The log-likelihood bit metric [26] is given as an input to the iterative decoder. The intervals for the AC protocol when the set of five turbo product codes are employed with QPSK modulation are given in Table 4.1.

According to the approximation suggested in Section 3.1.2 for QPSK modulation, the conditional distribution of the distance statistic given the channel state is a Gaussian

distribution with mean $\mu_D(j,k)/\mu$ and variance $\sigma_D^2(j,k)/2L_v\mu^2$. From the approximation, it follows that

$$\mathcal{Q}_{\mathrm{AC}}(n|j,k) \approx \Phi\left(\frac{\mu\gamma_{n-1}-\mu_D(j,k)}{\sigma_D(j,k)/\sqrt{2L_v}}\right) - \Phi\left(\frac{\mu\gamma_n-\mu_D(j,k)}{\sigma_D(j,k)/\sqrt{2L_v}}\right), \tag{4.8}$$

where $\mu_D(j,k)$ and $\sigma_D^2(j,k)$ are given by (3.10). Similar expressions can be obtained for $\mathcal{Q}_{\mathrm{AC}}(n|j,k)$ when the modulation is 16-QAM, 16-BOK, or 64-BOK by using the appropriate analytical expressions for the mean and variance of the demodulator statistic.

4.1.2 AMC protocol

The session throughput for the AMC protocol is given by (4.5). In what follows, we derive the analytical expressions for $\mathcal{Q}(n|j,k)$. In this section, we must consider three consecutive packets that we refer to as the previous packet, the current packet, and the next packet. The state of the channel for the previous packet influences the choice of modulation for the current packet, and that choice dictates which demodulator statistic is employed to determine the code-modulation combination for the next packet.

The conditional probability $\mathcal{Q}(n|j,k)$ is given by

$$\mathcal{Q}(n|j,k) = \sum_{v=1}^{n_m} P(\mathcal{M}_v|j,k)\mathcal{Q}(n|j,k,\mathcal{M}_v), \tag{4.9}$$

where $P(\mathcal{M}_v|j,k)$ is the conditional probability that the current packet uses modulation format $\mathcal{M}_v$ given that the channel state is (j,k), and $\mathcal{Q}(n|j,k,\mathcal{M}_v)$ is the conditional probability that $\mathcal{B}_n$ is chosen for the next packet given that the channel is in state (j,k) and the modulation format $\mathcal{M}_v$ is used for the current packet.

We first examine the conditional probability $P(\mathcal{M}_v|j,k)$. For the current packet that is transmitted when the channel is in state $S_2 = (j,k)$, the protocol selects the code-

modulation combination based on the previous channel state $S_1 = (l,m)$. A modulation format $\mathcal{M}_v$ is used for the current packet only if the protocol selects one of the code-modulation combinations that employ $\mathcal{M}_v$. So,

$$P(\mathcal{M}_v|j,k) = \sum_{l=0}^{J_f-1}\sum_{m=0}^{J_s-1} P[S_1 = (l,m)|S_2 = (j,k)]P[\mathcal{M}_v|S_1 = (l,m), S_2 = (j,k)], \quad (4.10)$$

where $P[S_1 = (l,m)|S_2 = (j,k)]$ is the conditional probability that the channel was in state (l,m) prior to being in state (j,k), and $P[\mathcal{M}_v|S_1 = (l,m), S_2 = (j,k)]$ is the conditional probability that $\mathcal{M}_v$ is used for the current packet given the previous and current states, S_1 and S_2 respectively. The choice of modulation for the current packet is based only the previous channel state. Therefore, the probability $P[\mathcal{M}_v|S_1 = (l,m), S_2 = (j,k)]$ does not depend on S_2 at all. Further, the conditional probability $P[\mathcal{M}_v|S_1 = (l,m), S_2 = (j,k)]$ can be expressed in terms of $\mathcal{Q}(n|l,m)$ to give

$$P(\mathcal{M}_v|j,k) = \sum_{l=0}^{J_f-1}\sum_{m=0}^{J_s-1} P[S_1 = (l,m)|S_2 = (j,k)] \sum_{x\in F(v)} \mathcal{Q}(x|l,m), \quad (4.11)$$

where $F(v)$ is the subset of $\{1,2,\ldots,N\}$ that contains the indices of all the code-modulation combinations that employ $\mathcal{M}_v$. Using Bayes' rule, we have

$$P[S_1 = (l,m)|S_2 = (j,k)] = \frac{q_1(j|l)q_2(k|m)\pi_l\pi'_m}{\pi_j\pi'_k}. \quad (4.12)$$

Using (4.12) in (4.11), we get

$$P(\mathcal{M}_v|j,k) = \sum_{l=0}^{J_f-1}\sum_{m=0}^{J_s-1} \frac{q_1(j|l)q_2(k|m)\pi_l\pi'_m}{\pi_j\pi'_k} \sum_{x\in F(v)} \mathcal{Q}(x|l,m), \quad (4.13)$$

Next, we examine the conditional probability $\mathcal{Q}(n|j,k,\mathcal{M}_v)$. For the AMC protocol,

we have

$$\mathcal{Q}(n|j,k,\mathcal{M}_v) = P(\Gamma_v \in \mathcal{I}_{v,n}|j,k,\mathcal{M}_v), \tag{4.14}$$

where Γ_v is the demodulator statistic for $\mathcal{M}_v$ when the channel is in state (j,k). The conditional probability can be determined from the conditional distribution of Γ_v given the channel state (j,k).

Using (4.13) and (4.14) in (4.9), we have

$$\mathcal{Q}(n|j,k) = \sum_{v=1}^{n_m} P(\Gamma_v \in \mathcal{I}_{v,n}|j,k,\mathcal{M}_v) \left(\sum_{l=0}^{J_f-1} \sum_{m=0}^{J_s-1} \frac{q_1(j|l)q_2(k|m)\pi_l\pi'_m}{\pi_j\pi'_k} \sum_{x\in F(v)} \mathcal{Q}(x|l,m) \right), \tag{4.15}$$

where $1 \le n \le N, 0 \le j \le J_f - 1, 0 \le k \le J_s - 1$. Also,

$$\sum_{n=1}^{N} \mathcal{Q}(n|j,k) = 1, \tag{4.16}$$

for each j and k. The system of linear equations in (4.15) and (4.16) can be solved to obtain the values of $\mathcal{Q}(n|j,k)$, $1 \le n \le N$, $0 \le j \le J_f - 1$, $0 \le k \le J_s - 1$. Using these values in (4.5) we can evaluate analytically the session throughput for the AMC protocol.

For our numerical results, the five binary turbo product codes are employed with four modulation formats 64-BOK ($\mathcal{M}_1$), 16-BOK ($\mathcal{M}_2$), QPSK ($\mathcal{M}_3$), and 16-QAM ($\mathcal{M}_4$). Bit-interleaved coded modulation [27] is employed to allow each error-control code to be used with each modulation format. This gives 20 possible code-modulation combinations, but we use only the subset of 11 combinations that was selected in [28]. The list of 11 code-modulation combinations from [28] is given in Table 4.2 and the corresponding adaptation intervals are given in Table 4.3.

Note that Γ_1 and Γ_2 are the ratio statistics for 64-BOK and 16-BOK respectively;

Combination $\mathcal{B}_n$	Modulation	Code, Rate
$\mathcal{B}_1$	$\mathcal{M}_1$, 64-BOK	$\mathcal{C}_1$, 0.236
$\mathcal{B}_2$	$\mathcal{M}_1$, 64-BOK	$\mathcal{C}_3$, 0.495
$\mathcal{B}_3$	$\mathcal{M}_1$, 64-BOK	$\mathcal{C}_5$, 0.793
$\mathcal{B}_4$	$\mathcal{M}_2$, 16-BOK	$\mathcal{C}_3$, 0.495
$\mathcal{B}_5$	$\mathcal{M}_3$, QPSK	$\mathcal{C}_1$, 0.236
$\mathcal{B}_6$	$\mathcal{M}_3$, QPSK	$\mathcal{C}_2$, 0.325
$\mathcal{B}_7$	$\mathcal{M}_3$, QPSK	$\mathcal{C}_3$, 0.495
$\mathcal{B}_8$	$\mathcal{M}_3$, QPSK	$\mathcal{C}_5$, 0.793
$\mathcal{B}_9$	$\mathcal{M}_4$, 16-QAM	$\mathcal{C}_3$, 0.495
$\mathcal{B}_{10}$	$\mathcal{M}_4$, 16-QAM	$\mathcal{C}_4$, 0.660
$\mathcal{B}_{11}$	$\mathcal{M}_4$, 16-QAM	$\mathcal{C}_5$, 0.793

Table 4.2: The set of code-modulation combinations for the AMC protocol.

Γ_3 and Γ_4 are the distance statistics for QPSK and 16-QAM respectively. In Chapter 3, we have approximated the distribution of Γ_v conditioned on the channel state by a Gaussian distribution with mean $\mu_v(j,k)$ and variance $\sigma_v^2(j,k)$. Recall that L_v is the number of modulation symbols in a packet that uses modulation format $\mathcal{M}_v$. For $v=1$ and 2, $\mu_v(j,k)=\mu_R(j,k)$ and $\sigma_v^2(j,k)=\sigma_R^2(j,k)/L_v$. For $v=3$ and 4, $\mu_v(j,k)=\mu_D(j,k)/\mu$ and $\sigma_v^2(j,k)=\sigma_D^2(j,k)/2L_v\mu^2$. From the Gaussian approximation, it follows that

$$\begin{aligned}\mathcal{Q}(n|j,k,\mathcal{M}_v) &= P(\Gamma_v \in \mathcal{I}_{v,n}|j,k,\mathcal{M}_v) \\ &\approx \Phi\left(\frac{\xi_{n-1}(v)-\mu_v(j,k)}{\sigma_v(j,k)}\right) - \Phi\left(\frac{\xi_n(v)-\mu_v(j,k)}{\sigma_v(j,k)}\right). \end{aligned} \tag{4.17}$$

Using (4.17) in (4.15) and solving the system of linear equations, we obtain the values of $\mathcal{Q}(n|j,k)$, for all n, j, and k. Subsequently, using the values of $\mathcal{Q}(n|j,k)$ in (4.5), we can calculate analytically the session throughput for the AMC protocol that uses the code-modulation combinations given in Table 4.2.

In what follows, we show that when the set of $N=11$ code-modulation combinations in Table 4.2 is used, $\mathcal{Q}(n|j,k)$ can be approximated by an expression that can be evaluated easily. The adaptation parameters $\xi_0(v),\ldots,\xi_N(v)$ for $1\le v\le 4$ are chosen em-

Combination $\mathcal{B}_n$	$\mathcal{I}_{1,n}$	$\mathcal{I}_{2,n}$	$\mathcal{I}_{3,n}$	$\mathcal{I}_{4,n}$
$\mathcal{B}_1$	$[0.723, 1)$	$[0.726, 1)$	$[1.467, \infty)$	$[2.663, \infty)$
$\mathcal{B}_2$	$[0.617, 0.723)$	$[0.704, 0.726)$	$[1.159, 1.467)$	$[2.018, 2.663)$
$\mathcal{B}_3$	$[0.472, 0.617)$	$[0.642, 0.704)$	$[0.909, 1.159)$	$[1.497, 2.018)$
$\mathcal{B}_4$	$[0.392, 0.472)$	$[0.574, 0.642)$	$[0.770, 0.909)$	$[1.173, 1.497)$
$\mathcal{B}_5$	$[0.328, 0.392)$	$[0.485, 0.574)$	$[0.691, 0.770)$	$[1.000, 1.173)$
$\mathcal{B}_6$	$[0.251, 0.328)$	$[0.376, 0.485)$	$[0.588, 0.691)$	$[0.783, 1.000)$
$\mathcal{B}_7$	$[0.172, 0.251)$	$[0.255, 0.376)$	$[0.434, 0.588)$	$[0.626, 0.783)$
$\mathcal{B}_8$	$[0.130, 0.172)$	$[0.204, 0.255)$	$[0.355, 0.434)$	$[0.567, 0.626)$
$\mathcal{B}_9$	$[0.100, 0.130)$	$[0.149, 0.204)$	$[0.276, 0.355)$	$[0.509, 0.567)$
$\mathcal{B}_{10}$	$[0.080, 0.100)$	$[0.123, 0.149)$	$[0.216, 0.276)$	$[0.449, 0.509)$
$\mathcal{B}_{11}$	$[0, 0.080)$	$[0, 0.123)$	$[0, 0.216)$	$[0, 0.449)$

Table 4.3: The adaptation intervals for the AMC protocol.

pirically with the goal of satisfying the following property: If the current channel state is (j,k), then the code-modulation combination $\mathcal{B}_{n_{j,k}}$ must be used for the next packet, where $s(n_{j,k}|j,k) = \max\{s(n|j,k) : 1 \leq n \leq N\}$. Since the protocol derives information about the channel state from the demodulator statistic, the protocol may not always select $\mathcal{B}_{n_{j,k}}$. The empirical choice of the adaptation parameters ensures that the selection of the code-modulation combination for the next packet is mostly independent of the modulation format used for the current packet. In other words, for a given channel state (j,k), the conditional probability $\mathcal{Q}(n|j,k,\mathcal{M}_v)$ is approximately the same for all $\mathcal{M}_v$. We verify this by examining the plots of $\mathcal{Q}(n|j,k,\mathcal{M}_v)$ for all n, $\mathcal{M}_v$, and a range of CENR values.

The conditional probability $\mathcal{Q}(n|j,k,\mathcal{M}_v)$ is plotted in Figure 4.1 for $n = 11$ as a function of CENR. Similar plots are shown for other values of n in Figures F.1a – F.3b (Appendix F). From these plots, we see that

$$\mathcal{Q}(n|j,k,\mathcal{M}_1) \approx \mathcal{Q}(n|j,k,\mathcal{M}_2) \approx \mathcal{Q}(n|j,k,\mathcal{M}_3) \approx \mathcal{Q}(n|j,k,\mathcal{M}_4). \tag{4.18}$$

The approximation seems to be accurate over all values of CENR.

Using (4.18) in (4.9), we can approximate $\mathcal{Q}(n|j,k)$, for our set of N = 11 code-

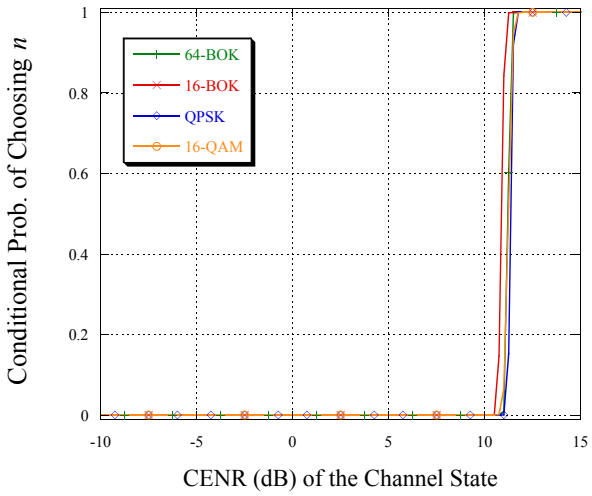

Figure 4.1: The conditional probability $\mathcal{Q}(n|j,k,\mathcal{M}_v)$ for $n = 11$.

modulation combinations, as

$$\begin{aligned}\mathcal{Q}(n|j,k) &\approx \mathcal{Q}(n|j,k,\mathcal{M}_v) \\ &\approx \Phi\left(\frac{\xi_{n-1}(v)-\mu_v(j,k)}{\sigma_v(j,k)}\right) - \Phi\left(\frac{\xi_n(v)-\mu_v(j,k)}{\sigma_v(j,k)}\right), \end{aligned} \tag{4.19}$$

where $v = 1,2,3$, or 4. Using the above approximation for $\mathcal{Q}(n|j,k)$ in (4.5), we can give an approximation to the session throughput for the AMC protocol.

4.2 Benchmark protocols

As a performance benchmark, we consider a hypothetical protocol that is provided with perfect state information for the next packet (PSI-N) [6,7]. The PSI-N protocol knows that the channel state will be (j,k) when the next packet is sent, and it chooses the code-modulation combination that maximizes the throughput achieved by the next packet. The

average throughput of the PSI-N protocol is

$$S_{\text{PSI-N}} = \frac{\sum_{j=0}^{J_f-1}\sum_{k=0}^{J_s-1} \pi_j \pi'_k s(n_{j,k}|j,k) N_t[n_{j,k}]}{\sum_{j=0}^{J_f-1}\sum_{k=0}^{J_s-1} \pi_j \pi'_k N_t[n_{j,k}]}, \tag{4.20}$$

where $s(n_{j,k}|j,k) = \max\{s(n|j,k) : 1 \le n \le N\}$. The PSI-N protocol is not practically realizable, but nevertheless it gives the highest throughput for the next packet that can be achieved with the set of error control codes and modulation formats available to the protocol.

We consider another hypothetical protocol that is provided with perfect state information for the preceding packet (PSI-P) [6, 7], which is more practical to obtain as opposed to PSI-N. We assume that the PSI-P protocol knows that the channel state was (j,k) for the preceding packet but does not know the parameters of the channel. The PSI-P protocol chooses for the next packet the code-modulation combination $\mathcal{B}_{n_{j,k}}$ such that $s(n_{j,k}|j,k) = \max\{s(n|j,k) : 1 \le n \le N\}$. The average throughput of the PSI-P protocol is

$$S_{\text{PSI-P}} = \frac{\sum_{j=0}^{J_f-1}\sum_{k=0}^{J_s-1} \pi_j \pi'_k \sum_{l=0}^{J_f-1}\sum_{m=0}^{J_s-1} q_1(l|j) q_2(m|k) s(n_{j,k}|l,m) N_t[n_{j,k}]}{\sum_{j=0}^{J_f-1}\sum_{k=0}^{J_s-1} \pi_l \pi'_k N_t[n_{j,k}]}. \tag{4.21}$$

Chapter 5

Performance Results

In this chapter, we demonstrate the accuracy of the analysis presented in Chapter 4. This is done by comparing the analytical calculations of the session throughput with the throughput obtained from a simulation of the demodulator-statistic based protocols and the Markov chain models of the fading channel and shadowing. We also compare the session throughput for the demodulator-statistic based protocols with the session throughput for the benchmark protocols.

5.1 AC protocol

We demonstrate the accuracy of the analysis presented in Section 4.1.1 for the AC protocol that uses QPSK modulation along with the set of five turbo-product codes given in Table 4.1. Our conclusions remain the same when 16-QAM, 16-BOK, or 64-BOK is used in place of QPSK modulation. The throughput obtained from the analytical results in (4.6) and (4.8) is compared with the throughput obtained from a simulation of the AC protocol and the Markov chain models of the fading channel and shadowing. In this section, the QPSK symbol-energy-to-noise ratio (QSENR) in dB is used as the measure of SNR. The

value of QSENR when there is no fading or shadowing is denoted by QSENR*.

For the fading Markov chain, we consider Nakagami-m fading [29] with $m=2.5$, which is approximately Rician fading with K-factor equal to 3.4. For $m=2.5$, the parameters of the fading Markov chain are as follows: The number of states is $J_f=12$, and the step size is $\Delta_1=1.25\,\text{dB}$. The throughput results are presented in Figure 5.1a for the Nakagami-m fading channel with $f_dT_s=0.02$, where f_d is the maximum Doppler frequency and T_s is the average time between two consecutive packet transmissions. Here, $f_dT_s=0.02$ represents relatively fast fading. In addition to the propagation losses due to Nakagami-m fading, we consider an additional intermittent 5 dB propagation loss due to shadowing that is experienced 4% of the time. Such a scenario is modeled by a two-state Markov chain with states 0 and 1 representing shadow losses of 0 dB and 5 dB respectively, and the transition probabilities given by $q_2(1|0)=0.002$ and $q_2(0|1)=0.01$. The steady-state probabilities for the Markov chain are $\pi_0'=0.9615$ and $\pi_1'=0.0384$. The throughput results are given in Figure 5.1b for the fading channel and the shadowing scenario considered.

The analytical calculations and the simulation results differ by less than 1.8% for almost all values of QSENR* in Figures 5.1a and 5.1b. Also shown in the Figures are the throughput results for the PSI-P and PSI-N protocols that use QPSK modulation with the same set of five turbo-product codes as the AC protocol. Although the AC protocol relies on demodulator statistics for it operation, it achieves throughput within 3% of the PSI-P protocol for almost all values of QSENR* in Figures 5.1a and 5.1b.

Similar results are shown for slower fading in Figure 5.2. When $f_dT_s=0.005$, the analytical calculations and the simulation results differ by less than 1.5% for almost all values of QSENR* in Figure 5.2. The AC protocol achieves throughput within 3% of the PSI-P protocol for almost all values of QSENR*.

The throughput of the PSI-N protocol is an upper bound on the performance of any practical adaptive coding protocol that uses QPSK modulation along with the set of five

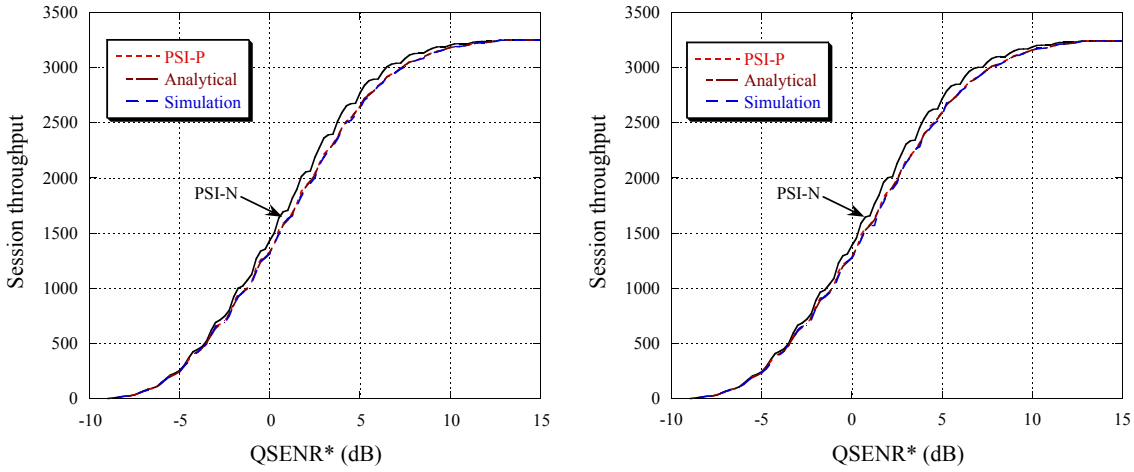

(a) No shadowing (b) Shadowing (5 dB loss 4% of the time)

Figure 5.1: Throughput of the adaptive coding protocols for Nakagami-m fading channel with $m = 2.5$ and $f_d T_s = 0.02$

turbo-product codes. The performance of the AC protocol is close to this upper bound in slower fading conditions. From Figures 5.1 and 5.1, we see that shadowing at the 5 dB level for only 4% of the time has negigible effect on the performance of either of the adaptive coding protocols.

5.2 AMC protocol

We demonstrate the accuracy of the analysis presented in Section 4.1.2 for the AMC protocol that uses the set of 11 code-modulation combinations given in Table 4.2. The throughput computed from (4.5) and solutions of (4.15) and (4.16) is compared with the throughput obtained from a simulation of the AMC protocol and the Markov chain models of the fading channel and shadowing. The accuracy of the approximation in (4.19) is also demonstrated. For all the results given in this section, the number of binary symbols per packet is $N_b = 4096$.

For the fading Markov chain, we consider Nakagami-m fading with $m = 1$, which

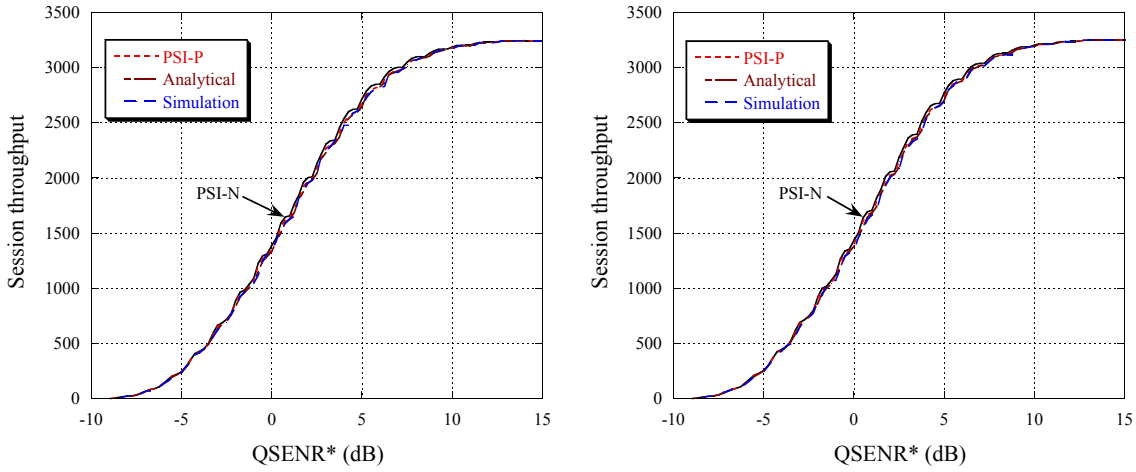

(a) No shadowing

(b) Shadowing (5 dB loss 4% of the time)

Figure 5.2: Throughput of the adaptive coding protocols for Nakagami-m fading channel with $m = 2.5$ and $f_d T_s = 0.005$

corresponds to Rayleigh fading, the most severe fading that is encountered in typical wireless channels. For $m = 1$, the parameters of the fading Markov chain are as follows: The number of states is $J_f = 12$, the step size is $\Delta_1 = 2$ dB. The value of CENR in the absence of fading and shadowing is denoted by CENR*. The value of CENR represented by each state in the Markov chain is an offset of CENR*. The throughput results are presented in Figure 5.3a for a Rayleigh fading channel with $f_d T_s = 0.02$.

Three different shadowing scenarios are considered. In shadowing scenario 1, a 10 dB shadow loss is experienced approximately 4% of the time. Scenario 1 is modeled by a two-state Markov chain with states 0 and 1 representing shadow losses of 0 dB and 10 dB respectively, and the transition probabilities given by $q_2(1|0) = 0.002$ and $q_2(0|1) = 0.05$. The steady-state probabilities are $\pi'_0 = 0.9615$ and $\pi'_1 = 0.0384$. In shadowing scenario 2, a 10 dB shadow loss is experienced approximately 17% of the time. Scenario 2 is modeled by a two-state Markov chain with states 0 and 1 representing shadow losses of 0 dB and 10 dB respectively, and the transition probabilities given by $q_2(1|0) = 0.002$ and $q_2(0|1) = 0.01$.

The steady-state probabilities are $\pi'_0 = 0.8333$ and $\pi'_1 = 0.1667$. In shadowing scenario 3, shadow losses of 5 dB and 10 dB are each experienced one-third of the time. Scenario 3 is modeled by a three-state Markov chain with states 0, 1, and 2 representing shadow losses of 0 dB, 5 dB, and 10 dB respectively, and the transition probability matrix is given by

$$q_2 = \begin{bmatrix} 0.8 & 0.2 & 0 \\ 0.2 & 0.6 & 0.2 \\ 0 & 0.2 & 0.8 \end{bmatrix}. \tag{5.1}$$

The steady-state probabilities are $\pi'_0 = \pi'_1 = \pi'_2 = 0.33$. The throughput results are given in Figure 5.3b–5.3d for the fading channel and the shadowing scenarios considered.

The analytical calculations and the simulation results differ by less than 4.8% for almost all values of CENR* in Figures 5.3a–5.3d. The analytical calculations using the approximation predict the simulation results nearly as well as the exact calculations. Also shown in the graphs are the throughput results for the PSI-P and the PSI-N protocols that employ the same set of code-modulation combinations as the AMC protocol. Although the AMC protocol relies on demodulator statistics for its operation, it achieves throughput within 8% of the PSI-P protocol for almost all values of CENR* in Figures 5.3a–5.3d.

Analogous results are shown for slower fading in Figures 5.4a–5.4d. When $f_d T_s = 0.005$, the analytical calculations and the simulation results differ by less than 5% for almost all values of CENR*. The AMC protocol achieves throughput within 8% of the PSI-P protocol for almost all values of CENR*. As expected, the performance of the AMC protocol is close to the PSI-N benchmark in slower fading conditions. From Figures 5.3 and 5.4, we see that shadowing at the 10 dB level for 4% of the time has very little effect on the performance of either of the protocols. The other shadowing conditions considered lead to degradation in the performance of the AMC protocol as well as the benchmark protocols.

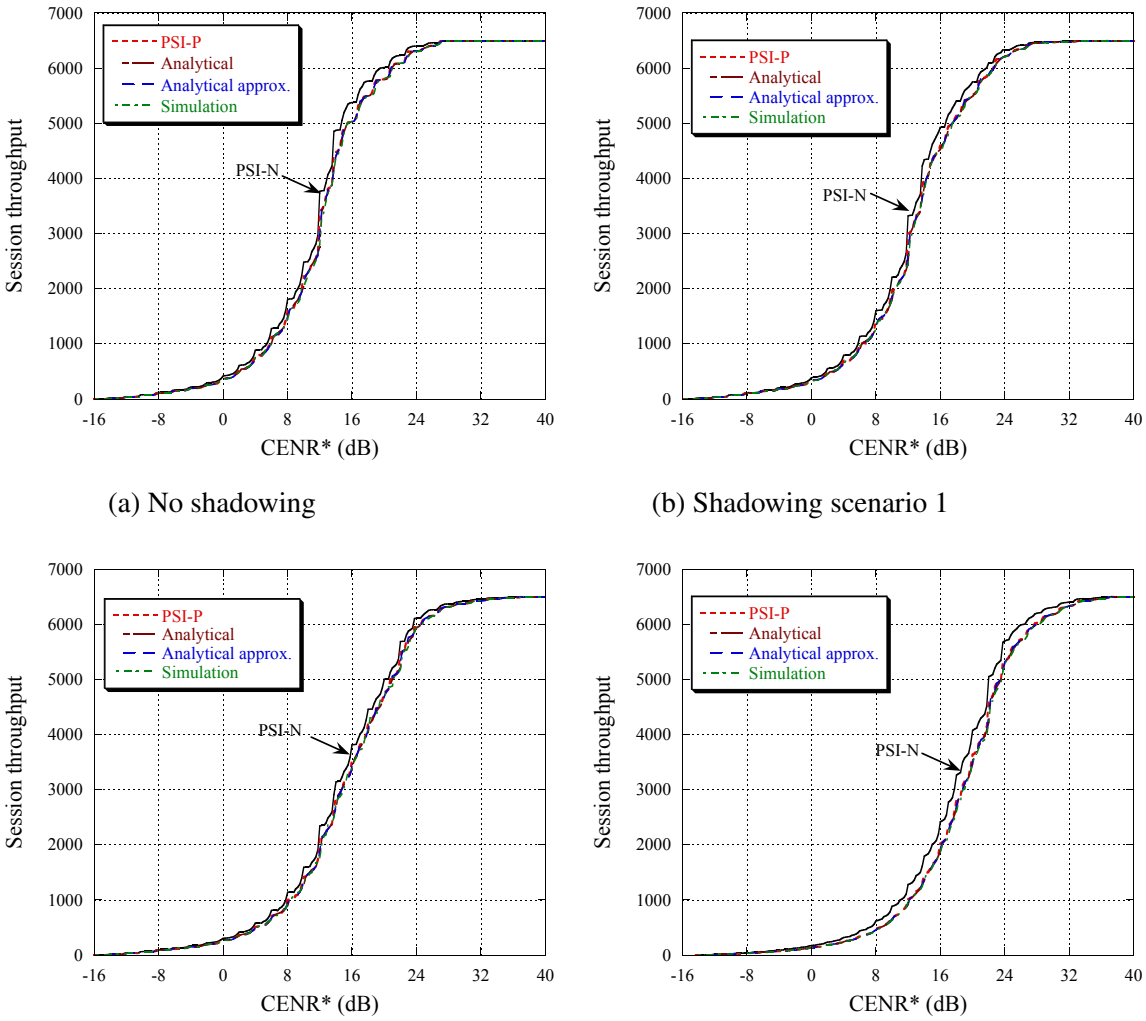

(a) No shadowing

(b) Shadowing scenario 1

(c) Shadowing scenario 2

(d) Shadowing scenario 3

Figure 5.3: Throughput of the adaptive modulation and coding protocols for a Rayleigh fading channel with $f_d Ts = 0.02$ and various shadowing scenarios

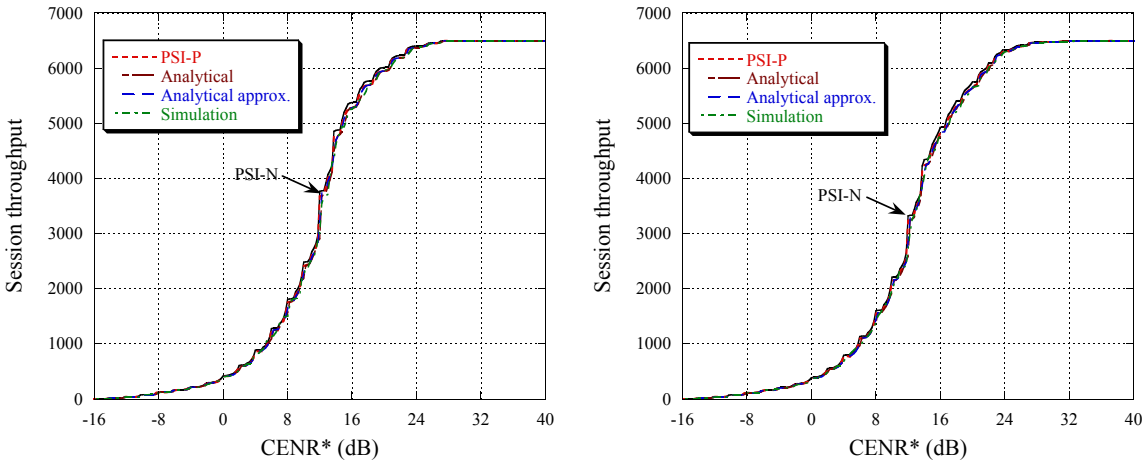

(a) No shadowing

(b) Shadowing scenario 1

(c) Shadowing scenario 2

(d) Shadowing scenario 3

Figure 5.4: Throughput of the adaptive modulation and coding protocols for a Rayleigh fading channel with $f_d T s = 0.005$ and various shadowing scenarios

Chapter 6

Conclusion

We have developed an analytical method to evaluate the throughput performance of two demodulator-statistic based adaptive protocols for channels with fading and moderate shadowing. To this end, the process by which the protocols select the code or code-modulation combination for a packet was statistically characterized in terms of the probability distribution of the demodulator statistics. The analytical calculations were found to be in good agreement with the throughput results obtained from simulations of the protocol and the channel for various fading and shadowing scenarios. We have demonstrated that the demodulator-statistic based adaptive protocols are able to track the channel variations and perform nearly as well as a hypothetical protocol that has perfect state information for the preceding packet. In our approach for performance analysis, no simulations of the fading process, the shadowing, or the Markov models for these phenomena were required; furthermore, neither the adaptive protocol nor the generation of adaptation statistics was simulated in our approach.

Appendices

Appendix A 16-QAM: 1-D Distance Distribution

In this appendix, we determine the probability distribution function of the 1-D distance for 16-QAM when the channel is in state (j,k). We assume that the data variable U takes values uniformly at random from the set $\{b_\kappa : \kappa = 0,\ldots,3\}$, where $b_\kappa = 3-2\kappa$. When $U = b_\kappa$, the correlator output Z is Gaussian with mean $b_\kappa\mu$ and variance σ^2. The 1-D distance D can be expressed as a function of the correlator output, $D = g(Z)$, where

$$g(z) = \min\{|z-3\mu, ||z-\mu|, |z+\mu|, |z+3\mu|\}.$$

The distribution of the 1-D distance for 16-QAM when the channel is in state (j,k) is

$$F_D(x|j,k) = \sum_{\kappa=0}^{3} \frac{1}{4} P(g(Z) \le x|j,k,b_\kappa), \tag{A.1}$$

where $P(g(Z) \le x|j,k,b_\kappa)$ is the conditional probability that $g(Z) \le x$ given that the channel state is (j,k) and the data variable is b_κ. Note that the function g is even-symmetric and the conditional density function of Z when the channel state is (j,k) and the data variable is b_κ satisfies the following property for $\kappa = 2,3$

$$f_Z(z|j,k,b_\kappa) = f_Z(-z|j,k,b_{3-\kappa}).$$

Using these properties of $g(z)$ and $f_Z(z|j,k,b_\kappa)$, we can show that for $\kappa = 2,3$

$$P(g(Z) \le x|j,k,b_\kappa) = P(g(Z) \le x|j,k,b_{3-\kappa}).$$

Hence, we have

$$F_D(x|j,k) = \frac{1}{2}\{P(g(Z) \le x|j,k,b_0) + P(g(Z) \le x|j,k,b_1)\}, \tag{A.2}$$

where $P(g(Z) \leq x|j,k,b_\kappa)$, $\kappa = 0,1$ is given by

$$P(g(Z) \leq x|j,k,b_\kappa) = \begin{cases} 0, & x \leq 0, \\ P(Z \in [-3\mu - x, -3\mu + x] \cup [-\mu - x, -\mu + x] & \\ \quad \cup [\mu - x, \mu + x] \cup [3\mu - x, 3\mu + x]|j,k,b_\kappa), & 0 < x \leq \mu, \\ P(Z \in [-3\mu - x, 3\mu + x]|j,k,b_\kappa), & x > \mu. \end{cases} \tag{A.3}$$

When the data variable is b_1, we have

$$P(g(Z) \leq x|j,k,b_1) = \begin{cases} 0, & x \leq 0, \\ 2\Phi\left(\frac{x}{\sigma}\right) + 2\Phi\left(\frac{x+2\mu}{\sigma}\right) + 2\Phi\left(\frac{x-2\mu}{\sigma}\right) & \\ \quad + \Phi\left(\frac{x+4\mu}{\sigma}\right) + \Phi\left(\frac{x-4\mu}{\sigma}\right) - 4, & 0 < x \leq \mu, \\ \Phi\left(\frac{x+2\mu}{\sigma}\right) + \Phi\left(\frac{x+4\mu}{\sigma}\right) - 1, & x > \mu. \end{cases} \tag{A.4}$$

When the data variable is b_0, we have

$$P(g(Z) \leq x|j,k,b_0) = \begin{cases} 0, & x \leq 0, \\ \Phi\left(\frac{x+2\mu}{\sigma}\right) + \Phi\left(\frac{x-2\mu}{\sigma}\right) + 2\Phi\left(\frac{x}{\sigma}\right) + \Phi\left(\frac{x+4\mu}{\sigma}\right) & \\ \quad + \Phi\left(\frac{x-4\mu}{\sigma}\right) + \Phi\left(\frac{x+6\mu}{\sigma}\right) + \Phi\left(\frac{x-6\mu}{\sigma}\right) - 4, & 0 < x \leq \mu, \\ \Phi\left(\frac{x}{\sigma}\right) + \Phi\left(\frac{x+6\mu}{\sigma}\right) - 1, & x > \mu. \end{cases} \tag{A.5}$$

Using (A.4) and (A.5) in (A.2), we can obtain the probability distribution function of the

1-D distance for 16-QAM as

$$F_D(x|j,k) = \begin{cases} 0, & x \leq 0, \\ 2\Phi\left(\frac{x}{\sigma}\right) + \frac{3}{2}\Phi\left(\frac{x+2\mu}{\sigma}\right) + \frac{3}{2}\Phi\left(\frac{x-2\mu}{\sigma}\right) + \Phi\left(\frac{x+4\mu}{\sigma}\right) & \\ \quad + \Phi\left(\frac{x-4\mu}{\sigma}\right) + \frac{1}{2}\Phi\left(\frac{x+6\mu}{\sigma}\right) + \frac{1}{2}\Phi\left(\frac{x-6\mu}{\sigma}\right) - 4, & 0 < x \leq \mu, \\ \frac{1}{2}(\Phi\left(\frac{x}{\sigma}\right) + \Phi\left(\frac{x+2\mu}{\sigma}\right) + \Phi\left(\frac{x+4\mu}{\sigma}\right) + \Phi\left(\frac{x+6\mu}{\sigma}\right)) - 1, & x > \mu. \end{cases} \tag{A.6}$$

Appendix B Identities

In this appendix, we prove two identities that are used to determine the mean and variance of the 1-D distances for QPSK and 16-QAM in Appendices C and D, respectively.

1. For real numbers a, b, and c,

$$\int_a^b (z-c\hat{\mu})\varphi(z;\hat{\mu},\sigma)dz = \frac{\sigma}{\sqrt{2\pi}}\left(\mathrm{e}^{\frac{-(a-\hat{\mu})^2}{2\sigma^2}} - \mathrm{e}^{\frac{-(b-\hat{\mu})^2}{2\sigma^2}}\right) - (c-1)\hat{\mu}\left\{\Phi\left(\frac{b-\hat{\mu}}{\sigma}\right) - \Phi\left(\frac{a-\hat{\mu}}{\sigma}\right)\right\}. \tag{B.1}$$

Proof. As $\varphi(z;\hat{\mu},\sigma) = (1/\sigma\sqrt{2\pi})\exp\{-(z-\hat{\mu})^2/2\sigma^2\}$, we have

$$\int_a^b (z-c\hat{\mu})\varphi(z;\hat{\mu},\sigma)dz = \int_a^b (z-\hat{\mu})\frac{1}{\sigma\sqrt{2\pi}}\mathrm{e}^{-\frac{(z-\hat{\mu})^2}{2\sigma^2}}dz - (c-1)\hat{\mu}\int_a^b \frac{1}{\sigma\sqrt{2\pi}}\mathrm{e}^{-\frac{(z-\hat{\mu})^2}{2\sigma^2}}dz.$$

Using change of variable $x = \frac{(z-\hat{\mu})^2}{2\sigma^2}$, we have

$$\begin{aligned}\int_a^b (z-c\hat{\mu})\varphi(z;\hat{\mu},\sigma)dz &= \int_{\frac{(a-\hat{\mu})^2}{2\sigma^2}}^{\frac{(b-\hat{\mu})^2}{2\sigma^2}} \frac{\sigma}{\sqrt{2\pi}}\mathrm{e}^{-x}dx - (c-1)\hat{\mu}\left\{\Phi\left(\frac{b-\hat{\mu}}{\sigma}\right) - \Phi\left(\frac{a-\hat{\mu}}{\sigma}\right)\right\} \\ &= \frac{\sigma}{\sqrt{2\pi}}\left(\mathrm{e}^{\frac{-(a-\hat{\mu})^2}{2\sigma^2}} - \mathrm{e}^{\frac{-(b-\hat{\mu})^2}{2\sigma^2}}\right) - (c-1)\hat{\mu}\left\{\Phi\left(\frac{b-\hat{\mu}}{\sigma}\right) - \Phi\left(\frac{a-\hat{\mu}}{\sigma}\right)\right\}.\end{aligned}$$

The values of a and b that are of interest while evaluating the mean of the 1-D distance are $-\infty$, $+\infty$, and multiples of μ.

2. For real numbers p and q,

$$\begin{aligned}\int_p^q (z-c\hat{\mu})^2\varphi(z;\hat{\mu},\sigma)dz = \int_p^q (z-\hat{\mu})^2\varphi(z;\hat{\mu},\sigma)dz + (c-1)^2\hat{\mu}^2\left\{\Phi\left(\frac{q-\hat{\mu}}{\sigma}\right) - \Phi\left(\frac{p-\hat{\mu}}{\sigma}\right)\right\} \\ + (2c-2)\hat{\mu}\frac{\sigma}{\sqrt{2\pi}}\mathrm{e}^{-\frac{(q-\hat{\mu})^2}{2\sigma^2}} + (2-2c)\hat{\mu}\frac{\sigma}{\sqrt{2\pi}}\mathrm{e}^{-\frac{(p-\hat{\mu})^2}{2\sigma^2}}.\end{aligned} \tag{B.2}$$

Proof.

$$\int_p^q (z-c\hat{\mu})^2 \varphi(z;\hat{\mu},\sigma)dz = \int_p^q (z-\hat{\mu})^2 \varphi(z;\hat{\mu},\sigma)dz + (c^2-1)\hat{\mu}^2 \int_p^q \varphi(z;\hat{\mu},\sigma)dz$$
$$- 2(c-1)\hat{\mu} \int_p^q z\varphi(z;\hat{\mu},\sigma)dz$$

Using (B.1), we have

$$\begin{aligned}\int_p^q (z-c\hat{\mu})^2 \varphi(z;\hat{\mu},\sigma)dz &= \int_p^q (z-\hat{\mu})^2 \varphi(z;\hat{\mu},\sigma)dz + (c^2-1)\hat{\mu}^2 \left\{\Phi\left(\frac{q-\hat{\mu}}{\sigma}\right) - \Phi\left(\frac{p-\hat{\mu}}{\sigma}\right)\right\} \\ &\quad - 2(c-1)\hat{\mu}\left(\frac{\sigma}{\sqrt{2\pi}}\left(e^{-\frac{(p-\hat{\mu})^2}{2\sigma^2}} - e^{-\frac{(q-\hat{\mu})^2}{2\sigma^2}}\right)\right. \\ &\quad \left. + \hat{\mu}\left\{\Phi\left(\frac{q-\hat{\mu}}{\sigma}\right) - \Phi\left(\frac{p-\hat{\mu}}{\sigma}\right)\right\}\right) \\ &= \int_p^q (z-\hat{\mu})^2 \varphi(z;\hat{\mu},\sigma)dz + (c-1)^2\hat{\mu}^2 \left\{\Phi\left(\frac{q-\hat{\mu}}{\sigma}\right) - \Phi\left(\frac{p-\hat{\mu}}{\sigma}\right)\right\} \\ &\quad + (2c-2)\hat{\mu}\frac{\sigma}{\sqrt{2\pi}}e^{-\frac{(q-\hat{\mu})^2}{2\sigma^2}} + (2-2c)\hat{\mu}\frac{\sigma}{\sqrt{2\pi}}e^{-\frac{(p-\hat{\mu})^2}{2\sigma^2}}.\end{aligned}$$

The unevaluated integral in the final expression is equal to σ^2 when $p=-\infty$ and $q=\infty$, and it is useful when deriving the expressions for the variance of the 1-D distance.

Appendix C QPSK: 1-D Distance Mean and Variance

In this appendix, we determine the mean and variance of the 1-D distance for QPSK when the channel is in state (j,k). We assume that the data variable U can take the value $+1$ or -1 with equal probability. When $U=\pm 1$, the correlator output Z is Gaussian with mean $\pm\mu$ and variance σ^2. The 1-D distance D can be expressed as a function of the correlator output Z as $D=g(Z)$, where $g(z)=\min\{|z-\mu|,|z+\mu|\}$.

C.1 Mean

The mean of the 1-D distance for QPSK when the channel is in state (j,k) is given by

$$E[D|j,k]=\frac{1}{2}\left(\int_{-\infty}^{\infty} g(z)f_Z(z|j,k,+1)+\int_{-\infty}^{\infty} g(z)f_Z(z|j,k,-1)\right), \tag{C.1}$$

where $f_Z(z|j,k,\pm 1)$ is the conditional density function of Z when the channel is in state (j,k) and $U=\pm 1$. Note that $f_Z(z|j,k,-1)=f_Z(-z|j,k,+1)$ and the function g is even-symmetric. Using these two properties, we can show that the conditional mean of the 1-D distance does not depend on the data variable U. Hence, without loss of generality, we assume that $U=+1$. Then, we have

$$E[D|j,k]=\int_{-\infty}^{\infty} g(z)f_Z(z|j,k,+1). \tag{C.2}$$

Let

$$E[D|j,k]=\sum_{i=1}^{4} I_i, \tag{C.3}$$

where $I_1=\int_{-\infty}^{-\mu}(-z-\mu)\varphi(z;\mu,\sigma)dz$, $I_2=\int_{-\mu}^{0}(z+\mu)\varphi(z;\mu,\sigma)dz$, $I_3=\int_{0}^{\mu}(-z+\mu)\varphi(z;\mu,\sigma)dz$, and $I_4=\int_{\mu}^{\infty}(z-\mu)\varphi(z;\mu,\sigma)dz$.

Identity (B.1) can be used to evaluate the integrals I_1 through I_4,

$$
\begin{aligned}
I_1 &= \frac{\sigma}{\sqrt{2\pi}} \mathrm{e}^{\frac{-2\mu^2}{\sigma^2}} - 2\mu\Phi\left(\frac{-2\mu}{\sigma}\right), \\
I_2 &= \frac{\sigma}{\sqrt{2\pi}} \left(\mathrm{e}^{\frac{-2\mu^2}{\sigma^2}} - \mathrm{e}^{\frac{-\mu^2}{2\sigma^2}}\right) + 2\mu\left\{\Phi\left(\frac{-\mu}{\sigma}\right) - \Phi\left(\frac{-2\mu}{\sigma}\right)\right\}, \\
I_3 &= \frac{\sigma}{\sqrt{2\pi}} (1 - \mathrm{e}^{\frac{-\mu^2}{2\sigma^2}}),
\end{aligned}
$$

and

$$
I_4 = \frac{\sigma}{\sqrt{2\pi}}.
$$

This gives

$$
E[D|j,k] = \sigma\sqrt{\frac{2}{\pi}} \left(1 - \mathrm{e}^{\frac{-\mu^2}{2\sigma^2}} + \mathrm{e}^{\frac{-2\mu^2}{\sigma^2}}\right) + 2\mu\left\{\Phi\left(\frac{-\mu}{\sigma}\right) - 2\Phi\left(\frac{-2\mu}{\sigma}\right)\right\}. \tag{C.4}
$$

C.2 Variance

Without loss of generality, we assume that $U = +1$. The second moment of the 1-D distance D when the channel is in state (j,k) is given by

$$
\begin{aligned}
E[D^2|j,k] &= \int_{-\infty}^{\infty} (g(z))^2 f_Z(z|j,k,+1)dz \\
&= \int_{-\infty}^{0} (z+\mu)^2 \varphi(z;\mu,\sigma)dz + \int_{0}^{\infty} (z-\mu)^2 \varphi(z;\mu,\sigma)dz.
\end{aligned}
$$

Using (B.2), we have

$$\begin{aligned} E[D^2|j,k] = &\int_{-\infty}^{0}(z-\mu)^2\varphi(z;\mu,\sigma)dz + 4\mu^2\Phi\left(\frac{-\mu}{\sigma}\right) \\ &- 4\mu\sigma\sqrt{\frac{1}{2\pi}}\mathrm{e}^{\frac{-\mu^2}{2\sigma^2}} + \int_{0}^{\infty}(z-\mu)^2\varphi(z;\mu,\sigma)dz \\ =&\sigma^2 + 4\mu^2\Phi\left(\frac{-\mu}{\sigma}\right) - 2\mu\sigma\sqrt{\frac{2}{\pi}}\mathrm{e}^{\frac{-\mu^2}{2\sigma^2}}. \end{aligned} \tag{C.5}$$

The variance of the 1-D distance when the channel is in state (j,k) can be determined by using (C.4) and (C.5),

$$\begin{aligned} \mathrm{Var}(D|j,k) &= E[D^2|j,k] - (E[D|j,k])^2 \\ &= \sigma^2 + 4\mu^2\Phi\left(\frac{-\mu}{\sigma}\right) - 2\mu\sigma\sqrt{\frac{2}{\pi}}\mathrm{e}^{\frac{-\mu^2}{2\sigma^2}} - (E[D|j,k])^2. \end{aligned} \tag{C.6}$$

Appendix D 16-QAM: 1-D Distance Mean and Variance

In this appendix, we determine the mean and variance of the 1-D distance for 16-QAM when the channel is in state (j,k). We assume that the data variable U takes values uniformly at random from the set $\{b_\kappa : \kappa = 0,\ldots,3\}$, where $b_\kappa = 3-2\kappa$. When $U = b_\kappa$, the correlator output Z is Gaussian with mean $b_\kappa\mu$ and variance σ^2. The 1-D distance D can be expressed as a function of the correlator output Z as $D = g(Z)$, where

$$g(z) = \min\{|z-3\mu, ||z-\mu|, |z+\mu|, |z+3\mu|\}.$$

D.1 Mean

The mean of the 1-D distance for 16-QAM when the channel is in state (j,k) is given by

$$\begin{aligned} E[D|j,k] &= \frac{1}{4}\sum_{\kappa=0}^{3} E[D|j,k,b_\kappa] \\ &= \frac{1}{4}\sum_{\kappa=0}^{3}\int_{-\infty}^{\infty} g(z) f_Z(z|j,k,b_\kappa)dz, \end{aligned} \tag{D.1}$$

where the third variable in the conditioning refers to $U = b_\kappa$. Note that the function g is even-symmetric and $f_Z(z|j,k,b_\kappa) = f_Z(-z|j,k,b_{3-\kappa})$ for $\kappa = 2,3$. We can show that

$$E[D|j,k,b_2] = E[D|j,k,b_1]$$

and

$$E[D|j,k,b_3] = E[D|j,k,b_0].$$

Hence, we have

$$E[D|j,k] = \frac{1}{2}\left(E[D|j,k,b_1] + E[D|j,k,b_0]\right). \tag{D.2}$$

Let

$$E[D|j,k,b_\kappa] = \sum_{h=1}^{4} I_h^{(\kappa)}, \tag{D.3}$$

where $\kappa \in \{0,1\}$, $I_1^{(\kappa)} = \int_{-\infty}^{-2\mu} |z+3\mu|\varphi(z;b_\kappa\mu,\sigma)dz$, $I_2^{(\kappa)} = \int_{-2\mu}^{0} |z+\mu|\varphi(z;b_\kappa\mu,\sigma)dz$, $I_3^{(\kappa)} = \int_{0}^{2\mu} |z-\mu|\varphi(z;b_\kappa\mu,\sigma)dz$, and $I_4^{(\kappa)} = \int_{2\mu}^{\infty} |z-3\mu|\varphi(z;b_\kappa\mu,\sigma)dz$. When $\kappa=1$, using (B.1) to evaluate the integrals, we obtain

$$\begin{aligned}
I_1^{(1)} =& -\int_{-\infty}^{-3\mu} (z+3\mu)\varphi(z;\mu,\sigma)dz + \int_{-3\mu}^{-2\mu} (z+3\mu)\varphi(z;\mu,\sigma)dz \\
=& -\frac{\sigma}{\sqrt{2\pi}}\left(\mathrm{e}^{-\infty} - \mathrm{e}^{-\frac{(-3\mu-\mu)^2}{2\sigma^2}}\right) - 4\mu\Phi\left(\frac{-3\mu-\mu}{\sigma}\right) \\
&+ \frac{\sigma}{\sqrt{2\pi}}\left(\mathrm{e}^{-\frac{(-3\mu-\mu)^2}{2\sigma^2}} - \mathrm{e}^{-\frac{(-2\mu-\mu)^2}{2\sigma^2}}\right) + 4\mu\left\{\Phi\left(\frac{-2\mu-\mu}{\sigma}\right) - \Phi\left(\frac{-3\mu-\mu}{\sigma}\right)\right\} \\
=& \frac{\sigma}{\sqrt{2\pi}}\mathrm{e}^{\frac{-8\mu^2}{\sigma^2}} - 4\mu\Phi\left(\frac{-4\mu}{\sigma}\right) + \frac{\sigma}{\sqrt{2\pi}}(\mathrm{e}^{\frac{-8\mu^2}{\sigma^2}} - \mathrm{e}^{\frac{-9\mu^2}{2\sigma^2}}) + 4\mu\left\{\Phi\left(\frac{-3\mu}{\sigma}\right) - \Phi\left(\frac{-4\mu}{\sigma}\right)\right\},
\end{aligned} \tag{D.4}$$

$$\begin{aligned}
I_2^{(1)} =& -\int_{-2\mu}^{-\mu} (z+\mu)\varphi(z;\mu,\sigma)dz + \int_{-\mu}^{0} (z+\mu)\varphi(z;\mu,\sigma)dz \\
=& \frac{\sigma}{\sqrt{2\pi}}\left(\mathrm{e}^{\frac{-2\mu^2}{\sigma^2}} - \mathrm{e}^{\frac{-9\mu^2}{2\sigma^2}}\right) - 2\mu\left\{\Phi\left(\frac{-2\mu}{\sigma}\right) - \Phi\left(\frac{-3\mu}{\sigma}\right)\right\} \\
&+ \frac{\sigma}{\sqrt{2\pi}}\left(\mathrm{e}^{\frac{-2\mu^2}{\sigma^2}} - \mathrm{e}^{\frac{-\mu^2}{2\sigma^2}}\right) + 2\mu\left\{\Phi\left(\frac{-\mu}{\sigma}\right) - \Phi\left(\frac{-2\mu}{\sigma}\right)\right\},
\end{aligned} \tag{D.5}$$

$$\begin{aligned}
I_3^{(1)} =& -\int_{0}^{\mu} (z-\mu)\varphi(z;\mu,\sigma)dz + \int_{\mu}^{2\mu} (z-\mu)\varphi(z;\mu,\sigma)dz \\
=& -\frac{\sigma}{\sqrt{2\pi}}\left(\mathrm{e}^{\frac{-\mu^2}{2\sigma^2}} - 1\right) + \frac{\sigma}{\sqrt{2\pi}}\left(1 - \mathrm{e}^{\frac{-\mu^2}{2\sigma^2}}\right),
\end{aligned} \tag{D.6}$$

and

$$
\begin{aligned}
I_4^{(1)} &= -\int_{2\mu}^{3\mu}(z-3\mu)\varphi(z;\mu,\sigma)dz+\int_{3\mu}^{\infty}(z-3\mu)\varphi(z;\mu,\sigma)dz \\
&= -\frac{\sigma}{\sqrt{2\pi}}\left(\mathrm{e}^{\frac{-2\mu^2}{\sigma^2}}-\mathrm{e}^{\frac{-\mu^2}{2\sigma^2}}\right)+2\mu\left\{\Phi\left(\frac{2\mu}{\sigma}\right)-\Phi\left(\frac{\mu}{\sigma}\right)\right\} \\
&\quad +\frac{\sigma}{\sqrt{2\pi}}\mathrm{e}^{\frac{-2\mu^2}{\sigma^2}}-2\mu\left\{1-\Phi\left(\frac{2\mu}{\sigma}\right)\right\}. \qquad \text{(D.7)}
\end{aligned}
$$

This gives

$$
\begin{aligned}
E[D|j,k,b_1] &= \sum_{h=1}^{4} I_h^{(1)} \\
&= \sigma\sqrt{\frac{2}{\pi}}\left(1-2\mathrm{e}^{\frac{-\mu^2}{2\sigma^2}}+2\mathrm{e}^{\frac{-2\mu^2}{\sigma^2}}+\mathrm{e}^{\frac{-8\mu^2}{\sigma^2}}-\mathrm{e}^{\frac{-9\mu^2}{2\sigma^2}}\right) \\
&\quad +2\mu\left(2\Phi\left(\frac{-\mu}{\sigma}\right)-4\Phi\left(\frac{-2\mu}{\sigma}\right)+3\Phi\left(\frac{-3\mu}{\sigma}\right)-4\Phi\left(\frac{-4\mu}{\sigma}\right)\right). \qquad \text{(D.8)}
\end{aligned}
$$

Similarly, when $\kappa=0$, we have

$$
\begin{aligned}
I_1^{(0)} =& -\int_{-\infty}^{-3\mu}(z+3\mu)\varphi(z;3\mu,\sigma)dz+\int_{-3\mu}^{-2\mu}(z+3\mu)\varphi(z;3\mu,\sigma)dz \\
=& -\frac{\sigma}{\sqrt{2\pi}}\left(\mathrm{e}^{-\infty}-\mathrm{e}^{-\frac{(-3\mu-3\mu)^2}{2\sigma^2}}\right)-6\mu\Phi\left(\frac{-3\mu-3\mu}{\sigma}\right) \\
&+\frac{\sigma}{\sqrt{2\pi}}\left(\mathrm{e}^{-\frac{(-3\mu-3\mu)^2}{2\sigma^2}}-\mathrm{e}^{-\frac{(-2\mu-3\mu)^2}{2\sigma^2}}\right)+4\mu\left\{\Phi\left(\frac{-2\mu-3\mu}{\sigma}\right)-\Phi\left(\frac{-3\mu-3\mu}{\sigma}\right)\right\} \\
=&\frac{\sigma}{\sqrt{2\pi}}\mathrm{e}^{\frac{-18\mu^2}{\sigma^2}}-6\mu\Phi\left(\frac{-6\mu}{\sigma}\right)+\frac{\sigma}{\sqrt{2\pi}}(\mathrm{e}^{\frac{-18\mu^2}{\sigma^2}}-\mathrm{e}^{\frac{-25\mu^2}{2\sigma^2}})+6\mu\left\{\Phi\left(\frac{-5\mu}{\sigma}\right)-\Phi\left(\frac{-6\mu}{\sigma}\right)\right\},
\end{aligned}
\tag{D.9}
$$

$$
\begin{aligned}
I_2^{(0)} =& -\int_{-2\mu}^{-\mu}(z+\mu)\varphi(z;3\mu,\sigma)dz+\int_{-\mu}^{0}(z+\mu)\varphi(z;3\mu,\sigma)dz \\
=&\frac{\sigma}{\sqrt{2\pi}}\left(\mathrm{e}^{\frac{-8\mu^2}{\sigma^2}}-\mathrm{e}^{\frac{-25\mu^2}{2\sigma^2}}\right)-4\mu\left\{\Phi\left(\frac{-4\mu}{\sigma}\right)-\Phi\left(\frac{-5\mu}{\sigma}\right)\right\} \\
&+\frac{\sigma}{\sqrt{2\pi}}\left(\mathrm{e}^{\frac{-8\mu^2}{\sigma^2}}-\mathrm{e}^{\frac{-9\mu^2}{2\sigma^2}}\right)+4\mu\left\{\Phi\left(\frac{-3\mu}{\sigma}\right)-\Phi\left(\frac{-4\mu}{\sigma}\right)\right\},
\end{aligned}
\tag{D.10}
$$

$$
\begin{aligned}
I_3^{(0)} =& -\int_{0}^{\mu}(z-\mu)\varphi(z;3\mu,\sigma)dz+\int_{\mu}^{2\mu}(z-\mu)\varphi(z;3\mu,\sigma)dz \\
=& -\frac{\sigma}{\sqrt{2\pi}}\left(\mathrm{e}^{\frac{-2\mu^2}{\sigma^2}}-\mathrm{e}^{\frac{-9\mu^2}{2\sigma^2}}\right)-2\mu\left\{\Phi\left(\frac{-2\mu}{\sigma}\right)-\Phi\left(\frac{-3\mu}{\sigma}\right)\right\} \\
&+\frac{\sigma}{\sqrt{2\pi}}\left(\mathrm{e}^{\frac{-2\mu^2}{\sigma^2}}-\mathrm{e}^{\frac{-\mu^2}{\sigma^2}}\right)+2\mu\left\{\Phi\left(\frac{-\mu}{\sigma}\right)-\Phi\left(\frac{-2\mu}{\sigma}\right)\right\},
\end{aligned}
\tag{D.11}
$$

and

$$
\begin{aligned}
I_4^{(0)} =& -\int_{2\mu}^{3\mu}(z-3\mu)\varphi(z;3\mu,\sigma)dz+\int_{3\mu}^{\infty}(z-3\mu)\varphi(z;3\mu,\sigma)dz \\
=& -\frac{\sigma}{\sqrt{2\pi}}\left(1-\mathrm{e}^{\frac{-\mu^2}{2\sigma^2}}\right)+\frac{\sigma}{\sqrt{2\pi}},
\end{aligned}
\tag{D.12}
$$

which gives

$$E[D|j,k,b_0] = \sum_{h=1}^{4} I_h^{(0)}$$
$$= \sigma\sqrt{\frac{2}{\pi}} \sum_{h=0}^{6} (-1)^h \mathrm{e}^{\frac{-h^2\mu^2}{2\sigma^2}} + 2\mu \sum_{h=1}^{6} (-1)^{h+1} h \Phi\left(\frac{-h\mu}{\sigma}\right). \tag{D.13}$$

Using (D.8) and (D.13) to evaluate (D.2) gives

$$\begin{aligned} E[D|j,k] = &\frac{\sigma}{\sqrt{2\pi}} \left(2 - 3\mathrm{e}^{\frac{-\mu^2}{2\sigma^2}} + 3\mathrm{e}^{\frac{-2\mu^2}{\sigma^2}} - 2\mathrm{e}^{\frac{-9\mu^2}{2\sigma^2}} + 2\mathrm{e}^{\frac{-8\mu^2}{\sigma^2}} - \mathrm{e}^{\frac{-25\mu^2}{\sigma^2}} + \mathrm{e}^{\frac{-18\mu^2}{\sigma^2}}\right) \\ &+\mu \left[3\Phi\left(\frac{-\mu}{\sigma}\right) - 6\Phi\left(\frac{-2\mu}{\sigma}\right) + 6\Phi\left(\frac{-3\mu}{\sigma}\right) - 8\Phi\left(\frac{-4\mu}{\sigma}\right)\right. \\ &\left.+5\Phi\left(\frac{-5\mu}{\sigma}\right) - 6\Phi\left(\frac{-6\mu}{\sigma}\right)\right], \end{aligned} \tag{D.14}$$

which can be written compactly as

$$E[D|j,k] = \frac{\sigma}{\sqrt{2\pi}} \left(2 + \sum_{h=1}^{6} (-1)^h \lceil (7-h)/2 \rceil \, \mathrm{e}^{\frac{-h^2\mu^2}{2\sigma^2}}\right) + \mu \sum_{h=1}^{6} h(-1)^{h+1} \lceil (7-h)/2 \rceil \, \Phi\left(\frac{-h\mu}{\sigma}\right). \tag{D.15}$$

D.2 Variance

Without loss of generality, we can assume that $U = b_0$ or $U = b_1$. The second moment of the 1-D distance D for 16-QAM when the channel is in state (j,k) is given by

$$E[D^2|j,k] = \frac{1}{2}\left(E[D^2|j,k,b_0] + E[D^2|j,k,b_1]\right). \tag{D.16}$$

Let

$$E[D^2|j,k,b_\kappa] = \sum_{h=1}^{4} J_h^{(\kappa)}, \tag{D.17}$$

where $\kappa \in \{0,1\}$, $J_1^{(\kappa)} = \int_{-\infty}^{-2\mu}(z+3\mu)^2\varphi(z;b_\kappa\mu,\sigma)dz$, $J_2^{(\kappa)} = \int_{-2\mu}^{0}(z+\mu)^2\varphi(z;b_\kappa\mu,\sigma)dz$, $J_3^{(\kappa)} = \int_0^{2\mu}(z-\mu)^2\varphi(z;b_\kappa\mu,\sigma)dz$, and $J_4^{(\kappa)} = \int_{2\mu}^{\infty}(z-3\mu)^2\varphi(z;b_\kappa\mu,\sigma)dz$. When $\kappa=1$, using (B.2) to evaluate the integrals, we obtain

$$J_1^{(1)} = \int_{-\infty}^{-2\mu}(z-\mu)^2\varphi(z;\mu,\sigma)dz + 16\mu^2\Phi\left(\frac{-3\mu}{\sigma}\right) - 8\mu\frac{\sigma}{\sqrt{2\pi}}e^{\frac{-9\mu^2}{2\sigma^2}}, \tag{D.18}$$

$$J_2^{(1)} = \int_{-2\mu}^{0}(z-\mu)^2\varphi(z;\mu,\sigma)dz + 4\mu^2\left\{\Phi\left(\frac{-\mu}{\sigma}\right) - \Phi\left(\frac{-3\mu}{\sigma}\right)\right\} - 4\mu\frac{\sigma}{\sqrt{2\pi}}e^{\frac{-\mu^2}{2\sigma^2}} + 4\mu\frac{\sigma}{\sqrt{2\pi}}e^{\frac{-9\mu^2}{2\sigma^2}}, \tag{D.19}$$

$$J_3^{(1)} = \int_0^{2\mu}(z-\mu)^2\varphi(z;\mu,\sigma)dz, \tag{D.20}$$

and

$$J_4^{(1)} = \int_{2\mu}^{\infty}(z-\mu)^2\varphi(z;\mu,\sigma)dz + 4\mu^2\left\{1-\Phi\left(\frac{\mu}{\sigma}\right)\right\} - 4\mu\frac{\sigma}{\sqrt{2\pi}}e^{\frac{-\mu^2}{2\sigma^2}}. \tag{D.21}$$

This gives

$$E[D^2|j,k,b_1] = \sigma^2 - \frac{\mu\sigma}{\sqrt{2\pi}}(8e^{\frac{-\mu^2}{2\sigma^2}} + 4e^{\frac{-9\mu^2}{2\sigma^2}}) + 4\mu^2\left(2\Phi\left(\frac{-\mu}{\sigma}\right) + 3\Phi\left(\frac{-3\mu}{\sigma}\right)\right). \tag{D.22}$$

Similarly, when $\kappa=0$, we have

$$J_1^{(0)} = \int_{-\infty}^{-2\mu} (z-3\mu)^2 \varphi(z;3\mu,\sigma)dz + 16\mu^2\Phi\left(\frac{-3\mu}{\sigma}\right) - 8\mu\frac{\sigma}{\sqrt{2\pi}}\mathrm{e}^{\frac{-9\mu^2}{2\sigma^2}}, \tag{D.23}$$

$$\begin{aligned} J_2^{(0)} = &\int_{-2\mu}^{0} (z-3\mu)^2 \varphi(z;3\mu,\sigma)dz + 16\mu^2\left\{\Phi\left(\frac{-3\mu}{\sigma}\right) - \Phi\left(\frac{-5\mu}{\sigma}\right)\right\} \\ &- 8\mu\frac{\sigma}{\sqrt{2\pi}}\mathrm{e}^{\frac{-9\mu^2}{2\sigma^2}} + 8\mu\frac{\sigma}{\sqrt{2\pi}}\mathrm{e}^{\frac{-25\mu^2}{2\sigma^2}}, \end{aligned} \tag{D.24}$$

$$\begin{aligned} J_3^{(0)} = &\int_{0}^{2\mu} (z-3\mu)^2 \varphi(z;3\mu,\sigma)dz + 4\mu^2\left\{\Phi\left(\frac{-\mu}{\sigma}\right) - \Phi\left(\frac{-3\mu}{\sigma}\right)\right\} \\ &+ 4\mu\frac{\sigma}{\sqrt{2\pi}}\mathrm{e}^{\frac{-9\mu^2}{2\sigma^2}} - 4\mu\frac{\sigma}{\sqrt{2\pi}}\mathrm{e}^{\frac{-\mu^2}{2\sigma^2}}, \end{aligned} \tag{D.25}$$

and

$$J_4^{(0)} = \int_{2\mu}^{\infty} (z-3\mu)^2 \varphi(z;3\mu,\sigma)dz, \tag{D.26}$$

which gives

$$\begin{aligned} E[D^2|j,k,b_0] = &\sigma^2 - \frac{4\mu\sigma}{\sqrt{2\pi}}(\mathrm{e}^{\frac{-\mu^2}{2\sigma^2}} + \mathrm{e}^{\frac{-9\mu^2}{2\sigma^2}} + \mathrm{e}^{\frac{-25\mu^2}{2\sigma^2}}) \\ &+ 4\mu^2\left(\Phi\left(\frac{-\mu}{\sigma}\right) + 3\Phi\left(\frac{-3\mu}{\sigma}\right) + 5\Phi\left(\frac{-5\mu}{\sigma}\right)\right). \end{aligned} \tag{D.27}$$

Using (D.22) and (D.27) in (D.16) gives the second moment when the channel state is (j,k),

$$\begin{aligned} E[D^2|j,k] = &\sigma^2 - \frac{\mu\sigma}{2\sqrt{2\pi}}(12\mathrm{e}^{\frac{-\mu^2}{2\sigma^2}} + 8\mathrm{e}^{\frac{-9\mu^2}{2\sigma^2}} + 4\mathrm{e}^{\frac{-25\mu^2}{2\sigma^2}}) \\ &+ 2\mu^2\left(3\Phi\left(\frac{-\mu}{\sigma}\right) + 6\Phi\left(\frac{-3\mu}{\sigma}\right) + 5\Phi\left(\frac{-5\mu}{\sigma}\right)\right). \end{aligned} \tag{D.28}$$

Using (D.15) and (D.28) to evaluate the variance when the channel is in state (j,k) gives

$$\begin{aligned}\mathrm{Var}(D|j,k) &= E[D^2|j,k] - (E[D|j,k])^2 \\ &= \sigma^2 - \frac{\mu\sigma}{2\sqrt{2\pi}}(13\mathrm{e}^{\frac{-\mu^2}{2\sigma^2}} + 8\mathrm{e}^{\frac{-9\mu^2}{2\sigma^2}} + 4\mathrm{e}^{\frac{-25\mu^2}{2\sigma^2}}) \\ &\quad + 2\mu^2\left(3\Phi\left(\frac{-\mu}{\sigma}\right) + 6\Phi\left(\frac{-3\mu}{\sigma}\right) + 5\Phi\left(\frac{-5\mu}{\sigma}\right)\right) - (E[D|j,k])^2. \quad \text{(D.29)}\end{aligned}$$

Appendix E BOK: Symbol Ratio Mean and Variance

The analytical expression for the mean of symbol ratio in (3.12) can be expressed in terms of repeated one-dimensional integrals. When ζ_1 is sent as the symbol, the conditional mean of the symbol ratio is

$$E[R|j,k,\zeta_1] = \sum_{i=2}^{K} A_i + \sum_{i=2}^{K} B_i + \sum_{i=2}^{K} \sum_{\substack{l=2 \\ l\neq i}}^{K} C_{i,l}, \tag{E.1}$$

where

$$A_i = \int_{-\infty}^{\infty} \int_{-|z_1|}^{|z_1|} \frac{|z_i|}{|z_1|} P\left(m_1(\mathbf{z}) = z_1, m_2(\mathbf{z}) = z_i \middle| j,k,\zeta_1\right) \phi(z_1; AT/2, N_0T/4)\, \phi(z_i; 0, N_0T/4) dz_i dz_1, \tag{E.2}$$

$$B_i = \int_{-\infty}^{\infty} \int_{-|z_i|}^{|z_i|} \frac{|z_1|}{|z_i|} P\left(m_1(\mathbf{z}) = z_i, m_2(\mathbf{z}) = z_1 \middle| j,k,\zeta_1\right) \phi(z_i; 0, N_0T/4) \phi(z_1; AT/2, N_0T/4) dz_1 dz_i, \tag{E.3}$$

and

$$C_{i,l} = \int_{-\infty}^{\infty} \int_{-|z_i|}^{|z_i|} \frac{|z_l|}{|z_i|} P\left(m_1(\mathbf{z}) = z_i, m_2(\mathbf{z}) = z_l \middle| j,k,\zeta_1\right) \phi(z_i; 0, N_0T/4) \phi(z_l; 0, N_0T/4) dz_l dz_i. \tag{E.4}$$

The analytical expression for A_i, $2<i<K$ can be expressed as

$$A_i = \int_{-\infty}^{\infty} \frac{1}{|z_1|}\phi(z_1;AT/2,N_0T/4) \int_{-|z_1|}^{|z_1|} |z_i|\phi(z_i;0,N_0T/4) \left[\int_{-|z_i|}^{|z_i|} \frac{1}{\sqrt{2\pi\sigma^2}} e^{-\frac{z^2}{2\sigma^2}} dz\right]^{K-2} dz_i dz_1. \tag{E.5}$$

With change of variables $x=(z_1-AT/2)/N_0T/4$ and $y=z_i/N_0T/4$, we obtain

$$A_i = \int_{-\infty}^{\infty} \frac{1}{\left|x+\sqrt{\frac{2\mathcal{E}_s}{N_0}}\right|} \frac{1}{\sqrt{2\pi}} e^{-\frac{x^2}{2}} \int_{-\left|x+\sqrt{\frac{2\mathcal{E}_s}{N_0}}\right|}^{\left|x+\sqrt{\frac{2\mathcal{E}_s}{N_0}}\right|} \frac{|y|}{\sqrt{2\pi}} e^{-\frac{y^2}{2}} \left[\int_{-|y|}^{|y|} \frac{1}{\sqrt{2\pi}} e^{-\frac{z^2}{2}} dz\right]^{K-2} dydx \tag{E.6}$$

$$= \int_{-\infty}^{\infty} \frac{1}{\left|x+\sqrt{\frac{2\mathcal{E}_s}{N_0}}\right|} \phi(x;0,1) \int_{-\left|x+\sqrt{\frac{2\mathcal{E}_s}{N_0}}\right|}^{\left|x+\sqrt{\frac{2\mathcal{E}_s}{N_0}}\right|} |y| \quad \phi(y;0,1)\,[2\Phi(|y|)-1]^{K-2}\,dydx, \tag{E.7}$$

where $\mathcal{E}_s = A^2T/2$. Similarly, we have

$$B_i = \int_{-\infty}^{\infty} \frac{1}{|x|}\phi(x;0,1) \int_{-|x|-\sqrt{\frac{2\mathcal{E}_s}{N_0}}}^{|x|-\sqrt{\frac{2\mathcal{E}_s}{N_0}}} \left|y+\sqrt{\frac{2\mathcal{E}_s}{N_0}}\right| \phi(y;0,1) \left[2\Phi\left(\left|y+\sqrt{\frac{2\mathcal{E}_s}{N_0}}\right|\right)-1\right]^{K-2} dydx \tag{E.8}$$

and

$$C_{i,l} = \int_{-\infty}^{\infty} \int_{-|x|}^{|x|} \frac{|y|}{|x|}\phi(x;0,1)\phi(y;0,1) \left[\Phi\left(|y|-\sqrt{\frac{2\mathcal{E}_s}{N_0}}\right)+\Phi\left(|y|+\sqrt{\frac{2\mathcal{E}_s}{N_0}}\right)-1\right] [2\Phi(|y|)-1]^{K-3}\,dydx. \tag{E.9}$$

Note that A_i, B_i, and $C_{i,l}$ do not depend on the subscripts. Also, the mean of the symbol ratio does not depend on the symbol that was sent. Hence, we have

$$E[R|j,k] = (K-1)A_2 + (K-1)B_2 + (K-1)(K-2)C_{2,3}. \tag{E.10}$$

Similarly, the second moment of the symbol ratio is given by

$$E[R^2|j,k] = (K-1)A_2' + (K-1)B_2' + (K-1)(K-2)C_{2,3}', \tag{E.11}$$

where

$$A_2' = \int_{-\infty}^{\infty} \frac{1}{\left|x+\sqrt{\frac{2\mathcal{E}_s}{N_0}}\right|^2}\phi(x;0,1) \int_{-\left|x+\sqrt{\frac{2\mathcal{E}_s}{N_0}}\right|}^{\left|x+\sqrt{\frac{2\mathcal{E}_s}{N_0}}\right|} |y|^2\phi(y;0,1)\left[2\Phi(|y|)-1\right]^{K-2}dydx, \tag{E.12}$$

$$B_2' = \int_{-\infty}^{\infty} \frac{1}{|x|^2}\phi(x;0,1) \int_{-|x|-\sqrt{\frac{2\mathcal{E}_s}{N_0}}}^{|x|-\sqrt{\frac{2\mathcal{E}_s}{N_0}}} \left|y+\sqrt{\frac{2\mathcal{E}_s}{N_0}}\right|^2 \phi(y;0,1)\left[2\Phi\left(\left|y+\sqrt{\frac{2\mathcal{E}_s}{N_0}}\right|\right)-1\right]^{K-2} dydx, \tag{E.13}$$

and

$$C_{2,3}' = \int_{-\infty}^{\infty}\int_{-|x|}^{|x|} \frac{|y|^2}{|x|^2}\phi(x;0,1)\phi(y;0,1) \left[\Phi\left(|y|-\sqrt{\frac{2\mathcal{E}_s}{N_0}}\right)+\Phi\left(|y|+\sqrt{\frac{2\mathcal{E}_s}{N_0}}\right)-1\right]\left[2\Phi(|y|)-1\right]^{K-3}dydx. \tag{E.14}$$

The variance of the symbol ratio is computed from (E.10) and (E.11) as

$$\mathrm{Var}(R|j,k) = E[R^2|j,k] - (E[R|j,k])^2 \tag{E.15}$$

Appendix F Plots

The remaining plots that support the approximation (4.18) of Section 4.1.2 are given here.

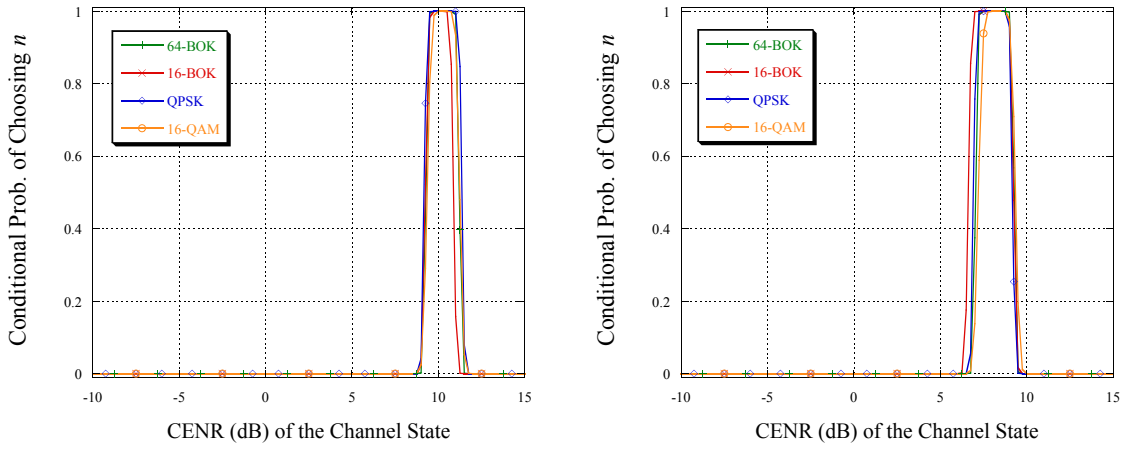

(a) $n = 10$ (b) $n = 9$

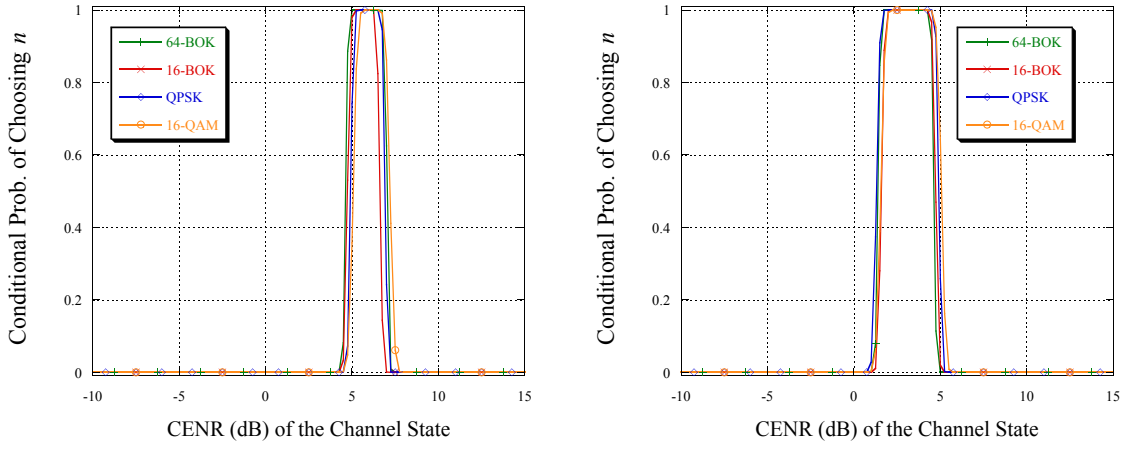

(c) $n = 8$ (d) $n = 7$

Figure F.1: The conditional probability $\Omega(n|j,k,\mathcal{M}_v)$ for (a) $n = 10$, (b) $n = 9$, (c) $n = 8$, and (d) $n = 7$.

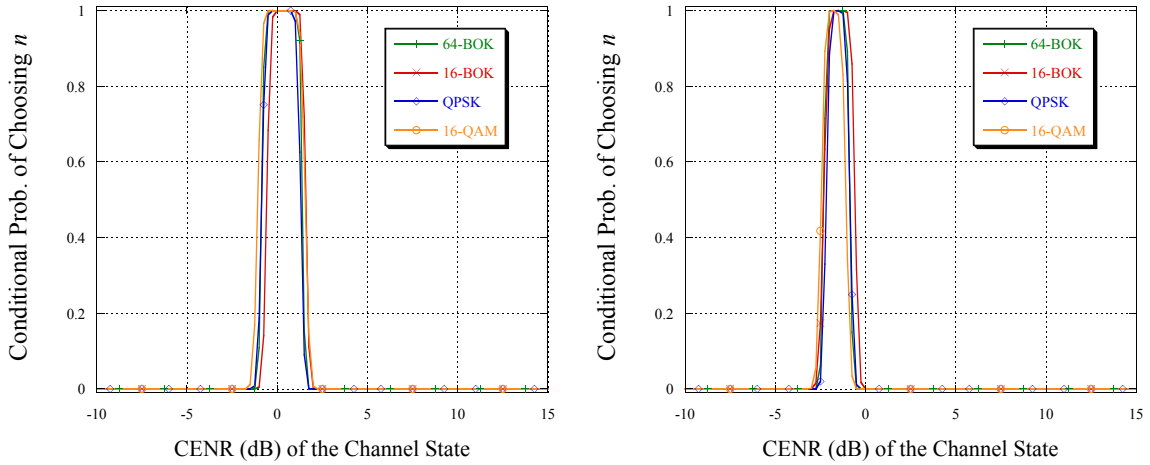

(a) $n = 6$ (b) $n = 5$

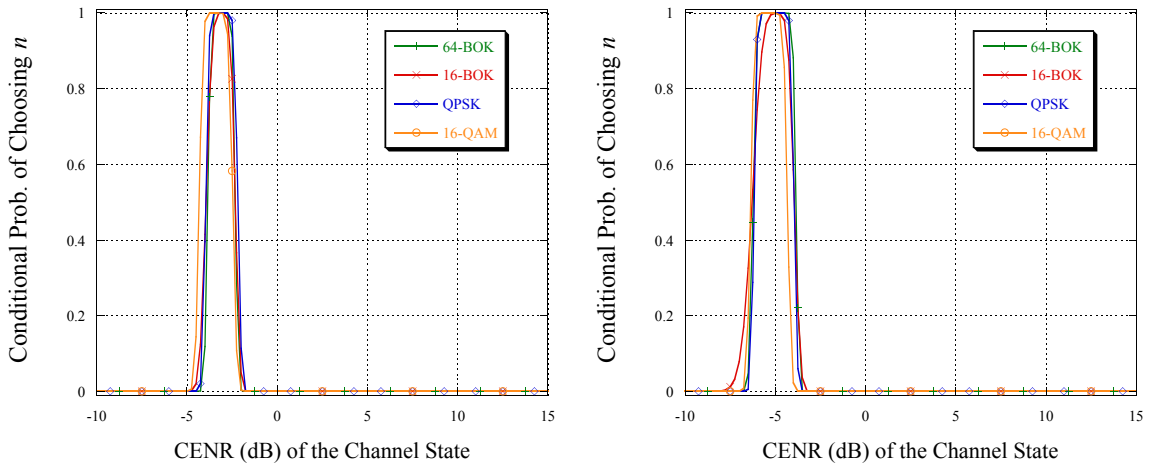

(c) $n = 4$ (d) $n = 3$

Figure F.2: The conditional probability $\Omega(n|j,k,\mathcal{M}_v)$ for (a) $n = 6$, (b) $n = 5$, (c) $n = 4$, and (d) $n = 3$.

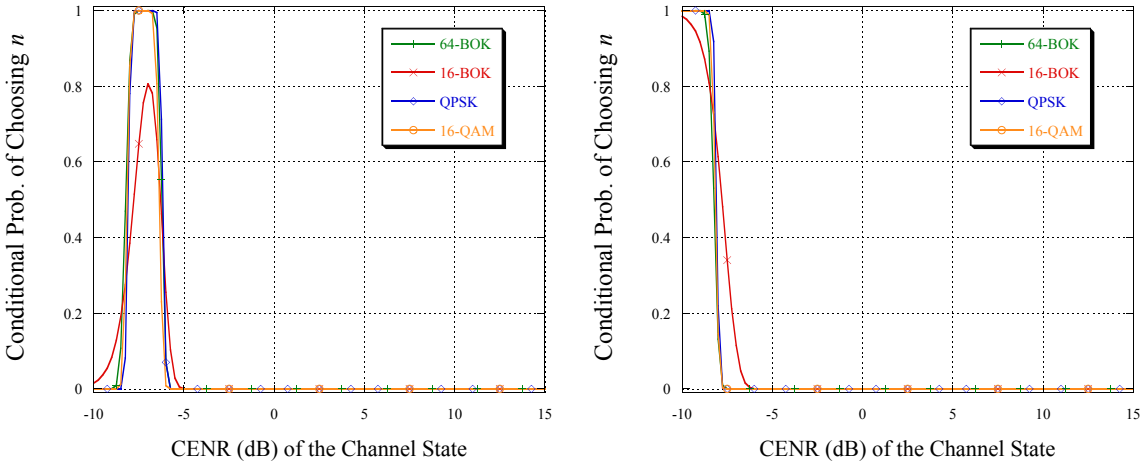

(a) $n = 2$ (b) $n = 1$

Figure F.3: The conditional probability $\mathcal{Q}(n|j,k,\mathcal{M}_v)$ for (a) $n = 2$ and (b) $n = 1$.

Bibliography

[1] A. Goldsmith, *Wireless communications*. Cambridge University Press, 2005.

[2] S. Vishwanath and A. Goldsmith, "Adaptive turbo-coded modulation for flat-fading channels," *IEEE Transactions on Communications*, vol. 51, no. 6, pp. 964–972, 2003.

[3] E. Armanious, D. D. Falconer, and H. Yanikomeroglu, "Adaptive modulation, adaptive coding, and power control for fixed cellular broadband wireless systems: some new insights," in *Proceedings of the 2003 IEEE Wireless Communications and Networking Conference*, vol. 1. IEEE, 2003, pp. 238–242.

[4] D. L. Goeckel, "Adaptive coding for time-varying channels using outdated fading estimates," *IEEE Transactions on Communications*, vol. 47, no. 6, pp. 844–855, 1999.

[5] Q. Liu, S. Zhou, and G. B. Giannakis, "Cross-layer combining of adaptive modulation and coding with truncated ARQ over wireless links," *IEEE Transactions on Wireless Communications*, vol. 3, no. 5, pp. 1746–1755, 2004.

[6] M. B. Pursley and J. S. Skinner, "Adaptive coding for frequency-hop transmission in mobile ad hoc networks with partial-band interference," *IEEE Transactions on Communications*, vol. 57, no. 3, pp. 801 –811, March 2009.

[7] M. B. Pursley and T. C. Royster IV, "Low-complexity adaptive transmission for cognitive radios in dynamic spectrum access networks," *IEEE Journal on Selected Areas in Communications*, vol. 26, no. 1, pp. 83–94, Jan. 2008.

[8] H. S. Wang and N. Moayeri, "Finite-state Markov channel—A useful model for radio communication channels," *IEEE Transactions on Vehicular Technology*, vol. 44, no. 1, pp. 163–171, February 1995.

[9] Q. Zhang and S. A. Kassam, "Finite-state Markov model for Rayleigh fading channels," *IEEE Transactions on Communications*, vol. 47, no. 11, pp. 1688–1692, November 1999.

[10] F. Babich and G. Lombardi, "A Markov model for the mobile propagation channel," *IEEE Transactions on Vehicular Technology*, vol. 49, no. 1, pp. 63–73, January 2000.

[11] A. Ramesh, A. Chockalingam, and L. B. Milstein, "A first-order Markov model for correlated Nakagami-m fading channels," in *Proceedings of the 2002 IEEE International Conference on Communications*, vol. 5, June 2002, pp. 3413–3417.

[12] V. Bhaskar, "Finite-state Markov model for lognormal, chi-square (central), chi-square (non-central), and K-distributions," *International Journal of Wireless Information Networks*, vol. 14, no. 4, pp. 237–250, 2007.

[13] J. M. Park and G. Hwang, "Mathematical modeling of Rayleigh fading channels based on finite state Markov chains," *IEEE Communications Letters*, vol. 13, no. 10, pp. 764–766, October 2009.

[14] M. A. Juang and M. B. Pursley, "New results on finite-state Markov models for Nakagami fading channels," in *Proceedings of the 2011 Military Communications Conference*, Nov. 2011, pp. 453 –458.

[15] J. D. Ellis, M. A. Juang, and M. B. Pursley, "Analytical evaluation of adaptive coding for Markov models of Nakagami fading," in *Proceedings of the 2012 Information Theory and Applications Workshop*, Feb. 2012, pp. 147 –151.

[16] M. B. Pursley, *Introduction to Digital Communications*. Upper Saddle River, NJ: Pearson Prentice Hall, 2005.

[17] A. J. Viterbi, "A robust ratio-threshold technique to mitigate tone and partial band jamming in coded MFSK systems," in *Proceedings of the 1982 Military Communications Conference (Boston)*, vol. 1, Oct. 1982, pp. 22.4–1 –22.4–5.

[18] M. B. Pursley and T. C. Royster IV, "High-rate direct-sequence spread spectrum with error-control coding," *IEEE Transactions on Communications*, vol. 54, no. 9, pp. 1693–1702, September 2006.

[19] T. C. Royster IV, "Protocols for dynamic spectrum access," Ph.D. dissertation, Clemson University, 2008.

[20] W. Feller, *An Introduction to Probability Theory and its Applications*. John Wiley & Sons, 2008, vol. 2.

[21] B. V. Gnedenko and A. N. Kolmogorov, *Limit Distributions for Sums of Independent Random Variables*. Reading, MA: Addison-Wesley, 1954 (Translated by K. L. Chung).

[22] V. V. Petrov, *Sums of Independent Random Variables*. Berlin: Springer-Verlag, 1975 (Translated from the Russian by A. A. Brown).

[23] K. L. Chung, *A Course in Probability Theory*, 2nd ed. Academic Press, New York, 1974.

[24] Advanced Hardware Architectures, Inc., Product Specification for AHA4501Astro 36 Mbits/sec Turbo Product Code Encoder/Decoder. Available: http://www.aha.com.

[25] S. Dolinar and D. Divsalar, "Weight distributions for turbo codes using random and nonrandom permutations," *JPL TDA Progress Report 42*, vol. 122, pp. 56–65, August 1995.

[26] S. Le Goff, A. Glavieux, and C. Berrou, "Turbo-codes and high spectral efficiency modulation," in *Proceedings of the 1994 IEEE International Conference on Communications*, 1994, pp. 645–649.

[27] G. Caire, G. Taricco, and E. Biglieri, "Bit-interleaved coded modulation," *IEEE Transactions on Information Theory*, vol. 44, no. 3, pp. 927–946, 1998.

[28] M. B. Pursley and T. C. Royster IV, "Protocols for adaptation in cognitive radios," in *Cognitive Radio Technology*, 2nd ed., B. A. Fette, Ed. Burlington, MA: Elsevier, 2009, pp. 689–721.

[29] M. Nakagami, "The m-distribution – A general formula of intensity distribution of rapid fading," *Statistical Method of Radio Propagation*, 1960.